Influence of the thermo-physical properties of pavement materials on the evolution of temperature depth profiles in different climatic regions

Matthew R Hall[1]*, Pejman Keikhaei Dehdezi[1, 2], Andrew R Dawson[2], James Grenfell[2], Riccardo Isola[2]

[1] Nottingham Centre for Geomechanics, Division of Materials, Mechanics and Structures, Faculty of Engineering, University of Nottingham, University Park, NG7 2RD, UK Tel: +44 (0) 115 846 7873, Fax: +44 (0) 115 951 3159, E-mail: matthew.hall@nottingham.ac.uk

[2] Nottingham Transport Engineering Centre, Division of Infrastructure and Geomatics, Faculty of Engineering, University of Nottingham, University Park, NG7 2RD, UK

* Correspondence author

Abstract

The paper summarizes the relative influence of different pavement thermo-physical properties on the thermal response of pavement cross-sections, and how their relative behaviour changes in different climatic regions. A simplified one-dimensional heat flow modelling tool was developed to achieve this using a finite difference solution method for studying the dynamic temperature profile within pavement constructions. This approach allows for a wide variety and daily varying climatic conditions to be applied, where limited or historic thermo-physical material properties are available, and permits the thermal behaviour of the pavement layers to be accurately modelled and modified. The model was used with available thermal pavement materials properties and with properties determined specifically for the study reported here. The pavement materials included in the study comprised both conventional bituminous and cementicious mixes as well as unconventional mixtures that allowed a wide range of densities, thermal conductivities, specific heat capacities and thermal diffusivities to be investigated. Initially, the model was validated against in-situ pavement data collected in the USA in five widely differing climatic regions. It was found to give results at least as good as others available from more computationally expensive approaches such as 2D and 3D FE

commercial packages. Then the model was used to compute the response for the same locations had the thermal properties been changed by using some of the unconventional pavement materials been used. This revealed that reduction of temperature range by several degrees was easily possible (with implications for reduction of rutting, fatigue and the Urban Heat Island effect) and that depth of penetration of peak temperatures was also achievable (with implications for winter freeze-thaw). However, the results showed that there was little opportunity to displace the peak temperatures in time.

Subject headings: Pavements; Heat transfer; Thermal diffusion; Temperature distribution; Numerical models

Nomenclature

a	absorptivity (-)
c_p	constant pressure specific heat capacity (J/kg K)
d	thickness of pavement/ground element (m)
h_c	total (or mean) convection heat transfer coefficient (W/m^2 K)
h_{rad}	total (or mean) radiation heat transfer coefficient, = $\varepsilon\sigma(T_0 + T_{sky})(T_0^2 + T_{sky}^2)$
i	counter for time step (i = 0 corresponding to specified initial condition)
$q_{absorbed}$	heat flux from surface absorbed solar radiation (W/m^2)
q_{solar}	heat flux from incident solar radiation (W/m^2)
L_c	characteristic length, i.e. area/perimeter (m)
m	number of nodal points (1, 2,… n)
Nu	Nusselt number for free and forced convection (-)
T_{sky}	sky temperature (K)
T_{air}	ambient air temperature (K)
T_{dp}	dew-point temperature (˚C)
T_0	absolute temperature of the surface (K)
T_m	temperature at nodal point m (K)

T_{surr}	surrounding temperature (K)
v_w	wind velocity (m/s)
α	thermal diffusivity (m^2/s)
σ	Stefan-Boltzmann constant = 5.668×10^{-8} ($W/m^2 K^4$)
ε	emissivity (-)
λ	dry state thermal conductivity (W/m K)
ρ_d	dry density (kg/m^3)

1. Introduction

Approximately half of the world's incoming solar energy is absorbed by the earth's surface (RETScreen 2005), and pavements comprise large areas of our infrastructure including roads, pedestrian pathways and parking areas. Temperature changes in pavements have been studied for many years since they have a significant impact on pavement performance under load-induced and thermal stresses and on service life. In flexible pavements (i.e. asphalt) the structural or load-carrying capacity of pavement varies with temperature since hot-mix asphalt (HMA) is a visco-elastic material (Ramadhan and Wahhab 1997; Marshall et al. 2001, Diefenderfer et al. 2002). In rigid pavements (i.e. concrete) temperature gradients across the concrete slab can cause structural defects such as warping and curling (Choubane and Tia 1992, Daiutolo 2003, Delatte 2008). Temperature variations in pavements can induce freeze-thaw cycles in the pavement which can often reduce their long-term stability (Dempsey & Thompson 1970). In addition, the significant contribution that pavements can make to the Urban Heat Island (UHI) is well known, and previous studies have attempted to predict this by numerically modelling near-surface temperature formation (Rosenfeld et al. 1998, Bretz et al. 1998).

In the UK, the temperature experienced in road pavements can vary between -8 °C and 60 °C, depending upon location and climate, and is usually above the ambient air temperature during the daytime and evening (Asaeda & Wake 1996). The US Strategic Highway Research Program (SHRP) established the Long Term Pavement Performance (LTPP) program in 1987. Lasting for a period of

more than ten years it involved thousands of test sections at hundreds of locations throughout the USA with complementary sections being built and monitored in other countries. Part of the study was the Seasonal Monitoring Program (SMP) with sixty four different test locations covering a highly diverse range of climatic conditions (Mohseni & Symons 1998). SMP data has since been used as a basis for validation of many pavement temperature prediction models (Dempsey & Thompson 1970, Rosenfeld et al. 1998, Solaimanian & Kennedy 1993, Hermansson 2000, Hermansson 2004). A significant problem is to understand how material selection and pavement design affect the temperature depth profile evolution, peak surface temperature, and responsiveness to climatic variables (e.g. solar irradiation, air temperature, surface wind velocity). Better understanding would allow intelligent design and material specification that could be tailored to match local climatic conditions. This could lead to improved performance and longevity of pavements, and enable better use of the heat as a low-grade energy source with existing technology, e.g. surface hot water collection. Enhanced shallow heat storage could be used in conjunction with ground source heat pump technology and road de-icing (van Bijsterveld & de Bondt 2002, de Bondt 2003, Carder 2007).

The objectives of this study are to use a predictive transient model to determine the behavioural sensitivity to pavement thermo-physical properties of

i) pavement surface temperature gain/loss

ii) temperature depth profile formation

iii) internal pavement temperature responsiveness in five contrasting climatic regions of the USA

The practical application of this research will be to provide generalised conclusions to help inform intelligent material selection and pavement design.

2. Thermo-physical properties of pavement materials

2.1 Past work

In unbound granular material (i.e. aggregates with some pore water), published data shows typical thermal conductivity figures of λ_{water} = 0.56 W/m K, λ_{air} = 0.026 W/m K and $\lambda_{mineral} \approx 3$ W/m K, varying somewhat with aggregate mineralogy (Yun & Santamarina 2008). Inter-particle contact and the degree of saturation play a critical role in heat transport phenomena in such materials. For the volume-averaged thermal conductivity of a representative sample of this material, the ordered sequence of magnitude is: $\lambda_{air} < \lambda_{dry\ soil} < \lambda_{water} < \lambda_{sat\ soil} < \lambda_{mineral}$ (Yun & Santamarina 2008). With reference to Figure 1, binder coatings increase the surface area at points of inter-particle contact, theoretically increasing heat flux within the material over that of the dry loose aggregates. However, the thermal conductivity of bitumen (as a binder) is relatively low, at $\lambda_{bitumen}$ = 0.15 - 0.17 W/m K (Hunter 2003), effectively acting as an insulative coating to aggregate particles. In contrast, hardened cement paste (HCP), which is found in concrete paving materials, has a thermal conductivity of approximately 0.8 – 0.9 W/m K (CES Edupack 2007). The thermo-physical properties of pavement materials can be selectively modified through the use of alternative aggregates, modified binders and/or void-filling conductive grouts. Further research is still needed to allow this to be done intelligently and in an accurately predictable manner. A review of existing published data for thermo-physical properties of standard pavement and sub-soil materials has been summarised in Table 1 for direct comparison with the new data presented in this study.

2.2 Present work

Independent experimental determination of thermo-physical properties, on a range of standard and modified pavement materials, was conducted for this study. This laboratory-based program of testing is now described.

Paving materials selected

Specimens of Dense Bitumen Macadam (DBM), a representative asphaltic road construction material, were produced using aggregates characterised by the particle size grading information provided in Table 2. A standard and a modified version of the DBM50 mix design was produced, the latter (potentially having enhanced thermal properties) used 34% vol. copper slag coarse aggregate (CA)

replacement and 35% vol. cooled iron shot dust replacement. Porous Asphalt (PA) mixes with 20%, 25% and 30% target air voids (TAV) along with a separate DBM mix with 4% TAV were produced using a 160/220 penetration grade bitumen binder and 10mm maximum aggregate size. It was anticipated that grouting PA would readily produce a paving material with increased thermal conductivity and bulk density (and hence also increased volumetric heat capacity) as a result of the reduction in air voids. This is a low cost alternative to the addition of expensive conductive fibre reinforcement materials. Grouting has the added advantages of improving long-term durability and stiffness, along with reduced rutting in surfaces that are exposed to high solar irradiation. Two pavement grade concrete mixes were also selected. The cross-section of a rigid pavement is most usually composed of Pavement Quality Concrete (PQC) on top of a low-strength Dry lean Concrete (DLC). The Defence Estates 2nd Edition of the *Guide to Airfield Pavement Design and Evaluation* (Defence Estates 2006) was used to provide the material specifications, and aggregate grading. Limestone aggregates were used due to their low coefficient of thermal expansion. The PQC mix design had a target 28-day compressive strength of 40 N/mm^2, whilst for the DLC mix the target strength was 20 N/mm^2. Both used 10/20 single sized limestone aggregate complying with BS EN 12620 (BSI 2002), '4mm down' natural sand, and high strength Portland cement (CEM I class, 52.5 N/mm^2).

Sample Preparation

The loose asphaltic mixes were compacted at a temperature of 130˚C into 305 × 305 × 50 mm slabs using a roller compactor. Some 20% TAV PA specimens had their voids grouted with three different grouts namely

- 100% CEM 1 class ordinary Portland cement,
- 80/20 %wt CEM1/densified silica fume (SF), and
- 80/20 %wt CEM 1/Class B Pulverised Fuel Ash (PFA).

The grout was prepared at 0.6 free water/cement ratio and poured onto the slabs whilst on a vibrating table to ensure full absorption. The freshly grouted slab specimens were cured at 95% RH ±5, and 20°

C ±2 prior to testing. PQC and DLC specimens were compacted using a vibration table and air cured for 24hr in laboratory conditions, before de-moulding and water curing for a period of 28 days at a temperature of 20°C ± 2.

Thermal Evaluation of Specimens

Thermal conductivity was determined using a computer-controlled P.A. Hilton B480 heat flow meter apparatus with downward vertical heat flow, which complies with ISO 8301 (ISO 1996). The slab specimens were placed inside the apparatus between a temperature-controlled hot plate and a water-cooled cold plate (both aluminium) connected to a thermo-electric chiller device. Steady state conditions were deemed to occur when the percentage variation in heat flux throughout the sample is $\leq$ 3%. The macadam/asphalt slabs were protected top and bottom with a square piece of thin aluminium foil to prevent bitumen sticking to the apparatus. The total test duration and determination of sampling interval period is calculated using a simple method that is dependent upon density, mean specific heat capacity and specimen thickness, as explained in a previous study (Hall & Allinson 2008a). For all test specimens, dry density, ρ_d was determined gravimetrically, and mean heat capacity was calculated using known values for particle density/specific gravity and specific heat capacity with reference to each mix design and its constituents (refer to method described in Hall & Allinson 2008b).

Results

The experimental data for the dry-state thermo-physical properties of these pavement materials is presented in Table 3. DBM materials generally have a similar Volumetric Heat Capacity (VHC) to Portland concrete but with lower thermal conductivity, due to the bituminous binder, and as a result are less thermally diffusive. The high porosity (low density) of PA materials significantly reduces both the thermal conductivity and thermal diffusivity, and the addition of cementicious grout gives an increase in VHC without significantly affecting diffusivity or conductivity. The use of high density alternative aggregates can significantly increase the VHC whilst maintaining a similar thermal conductivity.

3. Predictive modelling of pavement temperature depth profiles

Since roadways represent a relatively large surface area, by neglecting edge effects the predictive model can be reduced to a one-dimensional transient conduction model combined with a surface energy balance approach to predict the surface temperature under given climatic variables. This simply requires the cross-sectional construction detail of the pavement and the thermo-physical properties of the materials to be known. In reality, the heat transport mechanisms in pavement materials (concrete, asphalt or macadam) are complex, as depicted in Figure 1, and can involve radiation between particles, convection in the pores, phase change processes (latent energy transport) vaporisation and condensation process as well as freeze-thaw processes. Since pore sizes are negligibly small in relation to the volume of the structure under consideration, satisfactory modelling predictions can be made by reducing the complex heat transfer process to an equivalent conduction-only term (Brandl 2005).

The factors influencing the pavement surface energy balance, as well as the heat transport processes that occur within a pavement, are illustrated in Figure 2. The absorbed solar radiation on the pavement surface, $q_{absorbed}$ is simply equal to $a \cdot q_{solar}$, where 'a' is the absorptivity coefficient. The sensitivity of surface radiation absorption to pavement thermo-physical properties is dealt with in more detail in Section 4. Thermal (long-wave) radiation heat flux between the pavement surface and surrounding matter (i.e. the lower atmosphere, other buildings/objects) can be calculated as (Incropera et al. 2007):

$$q_{thermal} = \varepsilon\sigma\left(T_{surr}^4 - T_0^4\right) \qquad \text{Eq. 1}$$

T_{surr} is a hypothetical temperature that collectively represents the notional temperature of the surroundings objects and the lower atmosphere (air, clouds/water vapour), to which the surface can radiate heat. In the absence of dew point temperature data (T_{dp}), T_{surr} can be assumed as 6 K below the ambient dry bulb air temperature (Underwood & Yik 2004, Lienhard & Lienhard 2006). Despite that $T_{air} \neq T_{surr}$ some researchers have used the ambient air temperature alone to calculate long-wave radiation between pavement surfaces and the atmosphere (Hermansson 2004, Chen et al. 2008). The

modelling tool for this work uses the empirical Bliss equation which estimates the surrounding conditions in the form of a hypothetical 'sky temperature' (an approximation of T_{surr}) where (Gui et al. 2007, Chiasson et al. 2000, Yavuzturk et al. 2005):

$$T_{sky} = T_{air}(0.8 + \frac{T_{dp}}{250})^{0.25} \quad \text{Eq. 2}$$

There are also many empirical models that attempt to improve on the accuracy of the Bliss equation. The model in this paper was assessed using the empirical equations listed in Table 4. Figure 3 clearly shows that over a representative three-day period, when compared to the LTPP experimental data, using the Bliss equation gives the most accurate results and so this was used throughout the rest of the study.

Convection (natural and forced) accounts for heat transport at the pavement surface and the heat flux is simply calculated from $q_{convection} = h_c\,(T_{air} - T_0\,)$. The disparity between mean air velocity and near-surface air velocity, as a result of friction and uneven/rough surfaces, is often overlooked. The modelling tool for this work uses the empirical Jurges equation which estimates the mean convection heat transfer coefficient as a function of wind speed where (Niro et al. 2009, Bentz, 2000, CIBSE 2006):

$$h_c = 5.8 + 4.1 \cdot v_w \quad \text{Eq.10}$$

There are also many empirical models used by other researchers in order to calculate convective heat transfer at the pavement surface. The model in this paper was assessed using several other empirical equations as listed in Table 5 and a direct comparison between surface temperature predictions and LTPP experimental monitoring data has been performed. Figure 4 clearly shows that the Jurges' estimation of h_c provides the greatest level of accuracy over a representative 3-day period in two

contrasting climatic regions. This also suggests that surface convection heat transfer plays an important role in near-surface temperature profile formation.

One-dimensional vertical heat transport by transient conduction through the pavement can simply be modelled as a response to absorbed/desorbed energy at the pavement surface using an explicit form of the finite difference (FD) method. The cross-sectional pavement profile and the sub-soil beneath it can therefore be considered as a semi-infinite medium extending downward from $d = 0$ (pavement surface) to $d = x$, at which point $\Delta T \rightarrow 0$. In reality, at a critical depth (usually several meters) the ground temperature is approximately constant as a result of thermal mass and so is largely unaffected by heating/cooling cycles at the pavement surface. The numerical solution to the boundary condition at the pavement surface is then given by (Gui et al. 2007, Mrawira & Luca 2002):

$$\rho_d c_p \frac{\Delta d}{2} \frac{T_0^{i+1} - T_0^{i}}{\Delta t} = \mathrm{a} q_{solar} + h_c \left(T_{air} - T_0^{i}\right) + \varepsilon\sigma \left(T_{sky}^{4} - T_0^{4}\right) + \lambda \frac{T_1^{i} - T_0^{i}}{\Delta d} \qquad \text{Eq. 3}$$

The left side of Equation 3 gives the change in absorbed heat energy as a function of time, whilst the right hand side components (from left to right) represent heat energy from short-wave (solar) radiation gains, air convection gains/losses, long-wave radiation gains/losses, and fabric thermal conduction to/from $d = 0$. For interior nodes, the rate of heat conduction across a volume element of thickness Δd equals the change in the energy content of the element during a time interval Δt, therefore:

$$\lambda \frac{T^{i}_{m-1} - T^{i}_{m}}{\Delta d} - \lambda \frac{T^{i}_{m} - T^{i}_{m+1}}{\Delta d} = \rho_d c_p \left[\frac{T^{i+1}_{m} - T^{i}_{m}}{\Delta t}\right] \Delta d \qquad \text{Eq. 4}$$

A schematic diagram to identify the locations of mth node, m+1th node etc is shown in Figure 5. Solving for T^{i+1}_{m} gives:

$$T_m^{i+1} = \frac{\alpha \Delta t}{\Delta d^2}\left[T^i_{m-1} - 2T^i_m + T^i_{m+1}\right] + T^i_m \quad \text{Eq. 5}$$

where $\alpha = \frac{\lambda}{\rho_d c_p}$, the thermal diffusivity. The temperature of the interface nodes between layers of the pavement structure, e.g. the contact between surface layer and base layer, was derived from Equation 4 to give:

$$\lambda_1 \frac{T^i_{m-1} - T^i_m}{\Delta d_1} - \lambda_2 \frac{T^i_m - T^i_{m+1}}{\Delta d_2} = \rho_{d1} c_{p1}\left[\frac{T^{i+1}_m - T^i_m}{\Delta t}\right]\frac{\Delta d_1}{2} + \rho_{d2} c_{p2}\left[\frac{T^{i+1}_m - T^i_m}{\Delta t}\right]\frac{\Delta d_2}{2} \quad \text{Eq. 6}$$

This can then be solved for T^{i+1}_m to give:

$$T^{i+1}_m = \frac{\frac{\lambda_1}{\Delta d_1} T^i_{m-1} + \frac{\lambda_2}{\Delta d_2} T^i_{m+1} - \left[\frac{\lambda_1}{\Delta d_1} + \frac{\lambda_2}{\Delta d_2} - \frac{\rho_{d1} c_{p1} \Delta d_1}{2\Delta t} - \frac{\rho_{d2} c_{p2} \Delta d_2}{2\Delta t}\right] T^i_m}{\frac{\rho_{d1} c_{p1} \Delta d_1 + \rho_{d2} c_{p2} \Delta d_2}{2\Delta t}} \quad \text{Eq. 7}$$

The explicit method is not unconditionally stable, and the largest permissible value for the time step is limited by a stability criterion. In the case of transient one-dimensional heat conduction, the upper limit for all interior nodes is given by (Incropera et al. 2007, Holman 2002):

$$\Delta t \leq 0.5 \Delta d^2 / \alpha \quad \text{Eq.8}$$

and for surface nodes it can be expressed as (Gui et al. 2007):

$$\Delta t \leq \left(\frac{\rho_d c_p \Delta d^2}{2(h_{rad} \Delta d + h_c \Delta d + \lambda)}\right) \quad \text{Eq. 9}$$

In order to find the most restrictive value for Δt, first a value for Δd must be considered and then the maximum value of α (refer Tables 1 and 3) is inserted in Equation 8. In addition, the minimum value for ρ_d and c_p as well as a maximum logical value for h_{rad}, $h_{c,}$ and λ have to be inserted in Equation 9. The minimum (i.e. most restrictive) value for Δt should be used to provide the solution. In this study values of Δd=0.02m and of Δt = 30s were found to provide satisfactory stability for the range of typical thermo-physical properties in pavement materials (refer Tables 1 and 3) as well as climatic data.

The initial condition at t = 0 assumes a constant uniform temperature distribution to a depth of 2 m. Equations 5 to 7 are then solved by iteration in order to predicatively compute the temperature depth profile evolution at a given time interval. The environmental input parameters required for the model are hourly (or more frequently) solar irradiation, dry bulb air temperature, relative humidity (or dew point temperature) and mean wind velocity. The inputs were interpolated linearly across the hour period in order to achieve the 30 sec interval required for the model. In addition to surface absorptivity and surface emissivity, the pavement material thermo-physical properties required can be chosen from Tables 1 and 3 or experimentally determined.

4. Model sensitivity to pavement surface boundary conditions

The typical emissivity, ε, of concrete is 0.88 – 0.93 and for asphalt 0.85 – 0.93 (Incropera et al. 2007). Absorptivity (a) of a surface is the fraction of solar energy that is absorbed by the surface and it is normally a function of wavelength of the incoming radiation, surface colour, wetness, average temperature of pavement, and age of pavement surface (Solaimanian & Kennedy 1993). The absorptivity of a pavement surface generally decreases during its lifetime as the surface colour becomes lighter, and the reduction is more profound in asphalt pavements due to the high susceptibility of bitumen to aging (CIBSE 2006). For concrete pavement surfaces, ‘a’ values as low as 0.60 have been reported (Incropera et al. 2007) with a typical range being 0.65 – 0.80 (Bentz 2000, CIBSE 2006). Typical values for asphalt and macadam surfaces are 0.85 – 0.95 (Yavuzturk et al. 2005, CIBSE 2006). The values for pavement materials in general are lower than the typical range for

bare soil surfaces which are 0.85 – 0.92 (Holman 2002, Asaeda & Wake 1996). The relatively high sensitivity of near-surface temperature predictions to changes in 'a' can be seen in Figure 6 where the typical range in 'a' values for conventional pavement materials (concrete, asphalt and macadam) were used in the FD model and compared with LTPP experimental monitoring data. The highest solar irradiation test region (i.e. Arizona) was used in order to demonstrate maximum sensitivity. It can be seen that in this climate a difference of around 10 ˚C in the near-surface temperature could be achieved for the pavement materials used in this study. Note that the assumed 'a' value for this LTPP pavement was 0.88 which gave a good agreement between the predicted values and the measured values.

5. Temperature prediction and validation in different climatic regions

5.1 Validation against LTPP data

The FD model described earlier was used to predict pavement temperature profile evolution, at various different depths, in response to the climatic variables period. This was compared with actual recorded data provided by the SMP database of the LTPP project (US Department of Transportation – Federal Transport Administration, 2009). Five regions of contrasting climate were selected across the USA, as shown in Figure 7 along with the corresponding latitude and longitude. The climatic region and mean climatic variables for each test site are summarised and compared in Table 6. The predicted temperatures were modelled at three depth categories within the pavement; near-surface ($\leq$25mm), sub-surface (70-150mm) and mid-depth (200-350mm). The precise value for *d* in each of the three depth categories varied depending upon the precise position of the thermocouples at the five different LTPP project locations, as shown by the cross-sectional construction details of the test pavements in Figure 8. This shows the precise thermocouple location and thermo-physical material properties for each layer. The default absorptivity values used in the modelling were 0.85 for asphalt and 0.65 for concrete, taken as the mean average from published values (see above). For Arizona, the asphalt value was increased to 0.88 to account for the application of a dark surface sealant referred to in the SMP notes. In Montana, the concrete value was reduced to 0.60 to represent the formation of surface frost as proposed by Hermansson (Hermansson 2004). The comparison between the predicted near-surface,

sub-surface and mid-depth temperature profile evolution, and the actual SMP recorded data, was made over a 3-day representative period for each of the five test locations detailed above, see Figures 9 – 13.

5.2 Comparison with Enhanced Integrated Climatic Model (EICM)

An important way to validate the model is to compare it to other well established tools already available to industry and the scientific community. For this reason the authors have chosen to run two analyses to compare the results from the Enhanced Integrated Climatic Model, implemented within the Mechanistic-Empirical Pavement Design Guide (ME-PDG) with those of the presented model under two climatic scenarios selected from the LTPP database, i.e. 1-0101 (Alabama) and 31-3018 (Montana). Some input parameters that are required for our model could not be specified in the ME-PDG user interface and could, therefore, slightly decrease the accuracy of the simulations. The values used for these parameters were: Cloud Base Factor = 0.9, vapour pressure of air = 1.33mbar (minimum of range), a = 0.98 (newly constructed road), and surface emissivity = 0.93. The average daily values of air temperature, wind speed and pavement temperature with depth were all available in the climatic database for these sections, while the percentage of sunshine was only given as a monthly average and therefore, for the sake of the simulation, values were interpolated on a daily scale. Figures 14 and 15 show a comparison between the estimation of average monthly temperature at various depths (surface, 0.4m, 1m and 2m) performed using the two different models. The difference between predicted values from our model and EICM (within ME-PDG) was found to be between a mean value of 0.23˚C (Montana) and 0.55˚C (Alabama), which is less that the typical accuracy of a thermocouple used to record the experimental values (~ +/- 0.5˚C). It is not possible to directly compare the computational time for the two models in a fair way, since the ME-PDG must also perform structural analysis of the pavements as well as the thermal simulation, which requires several minutes (approximately 10 minutes for each of these simulations), whilst our model is coded in C# and can run the same simulations in less than one second.

The model presented here is intended to function as a simple research tool and performs to an acceptable standard and is typically accurate to within a 2 ˚C variation about the LTPP recorded

experimental value in all cases. This is at least the same level of accuracy as has been achieved in previous attempts to model pavement temperature profile evolution using a 1D transient conduction approach with dry state material thermo-physical properties (Dempsey & Thompson 1970, Rosenfeld et al. 1998, Solaimanian & Kennedy 1993, Hermansson 2000, Hermansson 2004), as well as when employing a 2-D FD model (Yavuzturk et al. 2005) and when using a 3D ANSYS FE model (Minhoto et al. 2006). The fast, simple, and computationally efficient Finite Difference (FD) approach was chosen for this study to enable rapid comparisons between multiple sets of material thermo-physical parameters and climatic variables without having to perform a detailed pavement structural design before each simulation, as with the EICM (ME-PDG). A hygrothermal (coupled heat & moisture) model would require extensive and detailed material properties characterisation for input parameters in terms of moisture-dependent thermal conductivity, moisture-dependent heat capacity, sorption/desorption isotherms, vapour permeability and liquid permeability coefficients. Pavement materials are non-homogenous and often only limited historical thermo-physical data (or core sample extraction) for existing highways is available. The authors propose that, given the accuracy of our simple model which requires only dry-state thermo-physical properties and climatic data and the scale of the pavement structure (thickness) and given the small additional accuracy gained from a hygrothermal modelling approach, that the research objective is very well satisfied without it.

6. Sensitivity analysis on the influence of material thermo-physical properties

Two categories were identified in order to define the 'thermal response' of a pavement structure to its ambient climatic conditions, in order to evaluate its sensitivity to changes in the material thermo-physical properties:

- Cyclic peak temperature variation as a function of depth (maximum/minimum)
- Amplitude suppression and time lag of peak temperature occurrence as a function of depth

For each category, the objective of the analysis was to determine how the controlled variation, for each of the achievable thermo-physical properties of pavement materials, can dominate any specific

changes in thermal response, and to what extent the magnitude of those changes are climate-specific. The outcomes of this analysis can be conveniently summarised under three sets of general conclusions, corresponding to the data presented in Figures 16 – 18.

Near-surface (0 – 25mm) peak temperatures and the range of peak temperature fluctuation (in a daily cycle) is inversely related to the thermal conductivity of the pavement surface layer, whilst at the same instance, mid-depth pavement temperatures are positively related, as shown by Figure 16. This behaviour occurs because heat flux away from the hot pavement surface (or from a hotter pavement core to a cooler surface) is increased when λ is high in the surface layer. The effect is greatest where surface energy gain is high, e.g. typically when short-wave or long-wave radiation gains, or convection gains, are high. We therefore see the greatest gains in Arizona and Nevada (up to 5˚C reduction in maximum , or 3˚C increase in minimum), a lesser extent in the humid/temperate climates of Alabama and Delaware (1˚C reduction in maximum, 2˚C increase in minimum), and only minimal changes in Montana (1˚C increase in minimum). Chen et al. (2008) used the NCHRP 1-37A Mechanistic Empirical Pavement Design Guide (ME-PDG) in order to show the relationship between pavement service life and maximum pavement surface temperature. They showed that, for the same traffic and the same materials, the life of the pavement can be extended by five years for a drop in temperature of 5°C. The opposite is true when low λ values are used, when surface temperatures are increased and mid-depth is decreased. In either case, separate analyses showed no significant effect on the time at which peak temperatures occur, i.e. no phase shift.

The VHC is positively related to the overall range of daily cycle temperature fluctuation and time-dependency of peak temperature occurrence, i.e. it governs the response time and sensitivity of material temperature to changes in the surface energy fluxes. Obviously the magnitude of peak temperature suppression about the mean (as a function of time) is directly proportional to diurnal temperature fluctuation, and largely independent of the mean temperature itself, as can be seen in Figure 17. Therefore, up to 4˚C suppression in maximum temperature is achievable in Delaware (~ 30˚C diurnal range), compared to only around 1˚C suppression in Montana (~ 12˚C diurnal range). In

all cases, the time lag in occurrence of both maximum and minimum peak temperatures is approximately 1 hour longer for the high VHC surface layer materials compared with those of low VHC. This suggests that whilst significant potential exists for optimising pavement surface layer materials in order to buffer peak temperatures, there is little potential for displacing the peak heat output relative to peak input time, e.g. so as to effect a reduction in urban temperatures during working hours.

The critical depth (d_{crit}) is defined by the point of convergence in daily cycle maximum/minimum temperature profiles and, from previous research conducted by the authors, is known to be positively related to the thermal diffusivity of pavement materials (Keikha et al. 2010). The implications are that the depth at which temperature stability is achieved can be controlled by layer thickness and material specification. For low diffusivity pavement surface materials, d_{crit} is approximately between 100 and 150mm regardless of climate, as shown by Figure 18. For high diffusivity pavement surface materials, d_{crit} is between, approximately, 250 and 400mm. It appears that d_{crit} is positively related to both the thermal diffusivity and thickness of the surface layer, and largely independent of climatic variables. Diffusivity simply represents the time-variant spread of heat energy and so determines the position at which temperature stability occurs in a pavement slab.

7. Conclusions and practical applications

It is concluded that various improvements can be made at the design stage of transport infrastructure by understanding the implications of the interaction between pavement design, the thermo-physical properties of the specified materials, and the ambient climatic conditions. Rutting is a particular problem in asphalt/macadam materials since they have a temperature-dependent Young's Modulus binder, i.e. they are bitumen-based. The ability to reduce surface temperatures in climates with high peak temperatures and short-wave radiation gains might be highly beneficial. In general terms, a pavement surface with high conductivity and low absorptivity will be cooler, as confirmed by our numerical predictions and the LTPP experimental data, and therefore less likely to suffer from rutting. Previous studies have also shown that when the maximum surface temperature is reduced by around

5ºC in hot climates such as Arizona and Nevada, the pavement service life can potentially be extended by up to five years. The same approach could be used to counteract the urban heat island effect as it would reduce heat emitted to the urban environment from the warm pavement surfaces, which is typically transported by long-wave radiation and natural convection.

A numerical modelling tool of 1D transient thermal conduction has been presented for predicting temperature profile evolution on pavement structures. It has been well validated in five contrasting climatic regions using accepted long-term monitoring data from the SMP programme as part of the LTPP project, and is as accurate as the best of comparable existing models. To improve prediction accuracy beyond 2˚C would require a hygrothermal model (fully coupled heat and moisture transport/storage) which necessitates highly detailed characterisation of the pavement material properties. In the longer term, the influence of moisture transport and storage on the model accuracy and climate-dependent response should be investigated to determine the influence on prediction accuracy in high rainfall regions. In these scenarios the simple model is unlikely to fully reflect the actual thermal processes of convection, radiation, and evaporation at the pavement surface, nor to accurately model heat and moisture movement inside the pavement. However, comparisons with models that do this, suggest that there is no significant improvement in accuracy for the wide range of contrasting climatic conditions tested in this study. A simple tool like this is easily used and applied by industry as part of pavement design protocol and material mix design specifications.

Warping usually effects rigid pavement layers, e.g. concrete surfaces or base layers, and is caused by the formation of a high temp gradient across the layer. This could be overcome by adjusting thermal diffusivity and therefore re-positioning the critical depth at a point immediately below the effected layer. Expansion and contraction cracking is a similar issue but is more likely in climates with very high diurnal temperature fluctuations, typically accompanied by high short-wave radiation gains at peak temperatures. By increasing the VHC of the surface layer to give, say, 3-4˚C temperature suppression (at peak) and around 6˚C reduction in total diurnal fluctuation (as demonstrated by the data presented here) the issue of cracking and loss of strength caused by thermal expansion/contraction

could be significantly reduced. In cold climates, the ability to prevent the pavement materials from getting so cold would be likely to have a measurable effect on extending fatigue life. In very cold climates a thick, low diffusivity pavement surface layer could provide a more stable temperature at shallower depths and thus reduce the freeze-thawing cycle and improve the pavement stability beneath the surface, i.e. reducing intermittent thaw softening (a problem that is expected to increase significantly in many northern climates as global warming prevents seasonal pavement freezing and leads to multiple freeze-thaw cycles). Further research is needed to see how pavement design and materials selection can be tailored to a specific location given the climatic variables of that region. Of course, benefits of reduced rutting and extended fatigue life will only be realized for materials having the same temperature susceptibility to these damage mechanisms. Much more work is required to balance mechanical properties and thermal properties – a balance that will need to be determined in a climate-specific framework.

Acknowledgements

The authors wish to acknowledge the financial support of this research by the Engineering and Physical Sciences Research Council (EPSRC) and East Midlands Airport. In addition, the authors wish to thank Robert Armitage and Daru Wityakamoto of the Scott Wilson Company, and Ayumi Hatakeyama, Dr David Allinson, and Peter Phillips at the University of Nottingham for their technical support, input and advice.

Table 1 – Previously published data for thermo-physical properties of pavement materials (dry state)

Specimen	ρ_d (kg/m³)	λ (W/m K)	C_p (J/kg K)	$\alpha \cdot 10^{-7}$ (m²/s)
Plain concrete (general) [a, m]	1600 - 3000	0.50 – 4.00	800 - 1200	1.4 - 20.8
Sub-soil (general) [d]	1400 - 2000	0.30 – 2.00	800 - 1100	1.4 - 17.8
PQC (general)	2339 [e]	1.20 [a]	1000 [a]	5.1
Crushed gravel/hardcore	2190 -2403 [e]	1.10 [b]	1000 [c]	4.6 - 5.0
Soil-aggregate mix	1650 [e]	1.00 [b]	960 [d]	6.3
Sub-soil	1782 -1906 [e]	0.80 [d]	1040 [d]	4.0 - 4.3
HMA [f – l]	1800 - 2500	0.50 - 2.50	900 - 2000	1.2 - 16.8

[a] (Mehta and Monteiro 2006), [b] (Côté & Konrad 2005), [c] (Dempsey & Thompson 1970), [d] (ASHRAE 1995), [e] (US Department of Transportation – Federal Transport Administration 2009), [f] (Luca & Mrawira 2005), [g] (Solaimanian & Bolzan 1993), [h] (Mrawira & Luca 2006), [i] (Mrawira & Luca 2002), [j] (Gui et al. 2007), [k] (Chadbourn et al. 1996), [l] (Zapata & Houston 2008), [m] (Lamond & Pielert 2006)

Table 2 – Aggregate type percentage passing from sieve analysis

Sieve size (mm)	14mm	10mm	6mm	dust	Filler
28	100	100	100	100	100
20	100	100	100	100	100
14	89.1	100	100	100	100
10	21.8	87.5	100	100	99.2
6.3	7	16.6	84.2	100	99.1
3.25	5.5	7.1	13.7	97.1	98.9
2.36	4.9	5.8	10	87.3	98.9
1.18	4.1	4.6	7.8	60.8	98.7
0.60	3.8	4.1	6.6	40.7	98.5
0.212	3	3	5.1	22.3	98
0.075	0.8	0.9	2.3	12.2	92.6

Table 3 – Thermo-physical properties of pavement materials (dry state)

Specimen	ρ_d **(kg/m³)**	λ **(W/m K)**	C_p **(J/kg K)**	$\alpha \cdot 10^{-7}$ **(m²/s)**
PQC	2319	1.11	858	5.6
DLC	2186	0.92	843	5.0
DBM 4% TAV 180/220 pen	2402	0.60	904	2.8
DBM 6% TAV 50 pen	2360	0.99	912	4.6
DBM w. Cu slag + Ferag	3296	0.92	720	3.9
PA 20% TAV 180/220 pen	2017	0.50	911	2.7
PA 25% TAV 180/220 pen	1925	0.47	911	2.7
PA 30% TAV 180/220 pen	1767	0.39	911	2.4
PA20% + CEM1 grout	2267	0.56	897	2.7
PA20% + CEM1/SF grout	2248	0.57	897	2.8
PA20% + CEM1/PFA grout	2322	0.55	897	2.6

Table 4 - Models used to calculate thermal (long-wave) radiation heat flux

Equations	Model	References
$T_{sky} = 5.53E\text{-}2 \cdot T_0^{1.5}$	Swinbank	Ramsey et al. 1981
$T_{sky} = (-3.015E9 + 1.22 \cdot T_0^4)^{0.25}$	Swinbank	Ramsey et al. 1981
$T_{sky} = T_0(1 - 0.261 \cdot \exp(-7.77E\text{-}4(273-T_0)^2))^{0.25}$	Idso & Jackson	Ramsey et al. 1981
$q=\varepsilon\sigma(4.8 + 0.075(T_{air} - 5))(T_0 - T_{air})$	HIPERPAVE	McCullough & Rasmussen 1998
$T_{sky} = \varepsilon_s^{0.25} \cdot T_{air}$ $\varepsilon_s = 0.787 + 0.764 \cdot \ln(T_{dp}/273) \cdot F_{cloud}$ $F_{cloud} = 1 + 0.024 \cdot N - 0.0035 \cdot N^2 + 0.00028 \cdot N^3$ $N = 0$ for clear sky and $N = 1$ for sky completely obscured by cloud	CONCTEMP	Minhoto et al. 2006

Table 5 - Models used to calculate convective heat flux at pavement surface

Equations	Model	References
$h_c = 698.24\left(0.00144 \cdot T_{avg}^{0.3} \cdot v_w^{0.7} + 0.00097\left(T_0 - T_{air}\right)^{0.3}\right)$ $T_{avg} = (T_0 + T_{air})/2$ v_w is between 0.8 to 8.5 m/s, and the surface temperature is between 6.7˚C and 27˚C	Vehrencamp	Vehrencamp 1953; Dempsey & Thompson 1970; Solaimanian & Kennedy 1993; Hermansson 2004; Mrawira & Luca 2002
$7.55 + 4.35 \cdot v_w$	Nicol	Palyvos 2007
$1.824 + 6.22 \cdot v_w$	Kimura	
$18.6 \cdot v_w^{0.605}$	ASHRAE	
$5.7 + 6.0 \cdot v_w$	Sturrock	
$16.15 \cdot v_w^{0.4}$	Loveday	

Table 6 – Mean climatic variables for the simulated test conditions in each of the five locations, data sourced from LTPP SMP (US Department of Transportation – Federal Transport Administration, 2009)

Location	**Zone***	**Climate type**		$T_{a,\,dry}$ (˚C)	RH (%)	q_{solar} (W/m^2)	v_w (m/s)
Arizona	3B	warm/hot - dry	Mean	27.6	25.6	296	2.3
			Max	35.3	64.1	957	4.6
			Min	17.2	5.7	0	0.6
Alabama	3A	warm - humid	Mean	25.8	79.8	265	1.7
			Max	33.5	99.7	954	4.2
			Min	21.0	42.1	0	0.2
Nevada	5B	cool - dry	Mean	27.9	22	306	2.8
			Max	37.9	56.1	967	7.7
			Min	13.5	9.0	0	0.5
Montana	6B	cold - dry	Mean	-13.5	62.5	77.4	0.7
			Max	-7.7	78.0	410	2.0
			Min	-20.0	34.7	0	0.1
Delaware	4A	mixed - dry	Mean	7.8	63.4	215.1	1.5
			Max	17.9	92.2	863	4.9
			Min	-1.6	30.2	0	0

* International climate zone definitions (ASHRAE, 2007)

Figure captions

Figure 1 – heat transport mechanisms between binder-coated aggregate particles, adapted from (Yun & Santamarina 2008)

Figure 2 – cross-sectional illustration of ground heat fluxes and surface energy balance, adapted from (Banks 2008)

Figure 3 – sensitivity comparison for long-wave radiation heat flux empirical formulae

Figure 4 – sensitivity comparison for near-surface temperature approximations due to convective heat transport

Figure 5 – a schematic diagram to identify the locations of mth node, m+1th node etc used in the finite difference model

Figure 6 – sensitivity comparison for near-surface temperature approximations under the range of pavement material absorptivity values

Figure 7 – regional climatic map of the USA showing the selected LTPP test site locations, adapted from (ASHRAE 2007). The two numbers given for each label are the latitude and longitude, respectively.

Figure 8 – cross-sectional designs of the five selected LTPP test pavement structures

Figure 9 – Three-day model validation for near-surface, sub-surface and mid-depth temperature profile evolution against LTPP experimental data for the Arizona test site

Figure 10 – Three-day model validation for near-surface, sub-surface and mid-depth temperature profile evolution against LTPP experimental data for the Alabama test site

Figure 11 – Three-day model validation for near-surface, sub-surface and mid-depth temperature profile evolution against LTPP experimental data for the Montana test site

Figure 12 – Three-day model validation for near-surface, sub-surface and mid-depth temperature profile evolution against LTPP experimental data for the Nevada test site

Figure 13 – Three-day model validation for near-surface, sub-surface and mid-depth temperature profile evolution against LTPP experimental data for the Delaware test site

Figure 14 – Comparison between simulated LTPP data (Montana) using our model and the ME-PDG EICM

Figure 15 – Comparison between simulated LTPP data (Alabama) using our model and the ME-PDG EICM

Figure 16 – The influence of high and low thermal conductivity pavement surface layers on temperature as a function of depth in each of the five test locations

Figure 17 – The influence of high and low volumetric heat capacity pavement surface layers on temperature as a function of time in each of the five test locations

Figure 18 – The influence of high and low thermal diffusivity pavement surface layers on temperature depth profile and critical depth in each of the five test locations

References

1. Asaeda, T. and Wake, V.T.C., (1996). "Heat Storage of Pavement and its Effect on the Lower Atmosphere." *Atmospheric Environment*, 30(3), 413-427.
2. ASHRAE, (2007). "ASHRAE Standard 90.1-2007 Energy Standard for Buildings Except Low-Rise Residential Buildings." American Society of Heating, Refrigeration and Air Conditioning Engineers Inc, Atlanta.
3. ASHRAE, (1995). "Commercial/institutional ground source heat pump engineering manual." American Society of Heating, Refrigerating and Air-Conditioning Engineers Inc, Atlanta.
4. Banks, D., (2008). "An Introduction to Thermogeology: Ground Source Heating and Cooling." Blackwell Publishing, Oxford.
5. Bentz, D. P., (2000). "A Computer Model to Predict the Surface Temperature and Time of Wetness of Concrete Pavements and Bridge Decks." *NISTIR 6551*, United States Department of Commerce, USA.
6. Brandl, H., (2005). "Energy Foundations and other thermo-active ground structures." *Geotechnique*, 56(2), 81-122.
7. Bretz, S., Akbari, H. and Rosenfeld, A. H., (1998). "Practical Issues for Using Solar-Reflective Materials to Mitigate Urban Heat Islands." *Atmospheric Environment*, 32(1), 95-101.
8. BSI, (2005). "BS 4987-1:2005 Coated Macadam (Asphalt Concrete) for Roads and Other Paved Areas - Specification for Constituent Materials and for Mixtures." British Standards Institute, London.
9. BSI, (2002). "BS EN 12620:2002 Aggregates for Concrete." British Standards Institute, London.
10. Carder, D. R., Barker, K. J., Hewitt, M. G., Ritter, D., and Kiff, A., (2007). "Performance of an inter-seasonal heat transfer facility for collection, storage, and re-use of solar heat from the road surface." *Transport Research Laboratory (TRL)*, Published Project Report PPR 302.
11. CES Edupack, (2007). "Cambridge Engineering Selector: Materials and Processes Database" [software], Granta Design, Cambridge

12. Chadbourn, B. A., Luoma, J. A., Newcomb, D. E., and Voller, V. R., (1996). "Consideration of Hot-Mix Asphalt Thermal Properties During Compaction." *STP 1299* American Society for Testing and Materials (ASTM), Philadelphia, 127–146.
13. Chen, B. L., Bhowmick, S., and Mallick, R. B., (2008). "Harvesting Energy from Asphalt pavements and reducing the heat island effect". Draft-2, White Paper-1. Available online at: http://users.wpi.edu/~rajib/Draft-2White-Paper-on-Reduce-Harvest-Heat-from-Pavements-Nov-2008.pdf.
14. Chiasson, A. D., Spitler, J. D., Rees, S. J., and Smith, M. D., (2000). "A Model for Simulating the performance of a Pavement Heating System as a Supplemental Heat Rejecter with Closed-Loop Ground-Source Heat Pump Systems." *J. Solar Energy Eng.*, 122(4), 183–191.
15. Choubane, B. and Tia, M., (1992). "Nonlinear Temperature Gradient Effect on Maximum Warping Stresses in Rigid Pavements." *Transportation Res. Record: J. Transportation Res. Board*, 1370, 11–19.
16. CIBSE, (2006). "Guide A: Environmental design – 7th Edition." Chartered Institute of Building Services Engineers, London
17. Côté, J. & Konrad, J. M., (2005). "Thermal Conductivity of Base-Course Materials." *Canadian Geotechnical Journal*, 42(2), 443-458.
18. Daiutolo, H., (2003). "Control of Slab Curling in Rigid Pavements at the FAA National Airport Pavement Test Facility (NAPTF)." Available online at: http://www.airtech.tc.faa.gov/NAPTF/Downloads/CC2%20Curling%20APT08.pdf.
19. de Bondt AH., (2003). "Generation of Energy Via Asphalt Pavement Surfaces." Asphaltica Padova, Netherland, Available online at: http://www.roadenergysystems.nl/pdf/Fachbeitrag%20in%20OIB%20%20de%20Bondt%20-%20English%20version%2013-11-2006.pdf.
20. Defence Estates, (2006). "A Guide to Airfield Pavement Design and Evaluation – 2nd Edition." Ministry of Defence: Defence Estates, Sutton Coldfield.
21. Delatte, N., (2008). "Concrete Pavement Design, Construction, and Performance." Taylor & Francis, London.

22. Dempsey, B. J. & Thompson, M. R., (1970), "A Heat-Transfer Model for Evaluating Frost Action Temperature-Related Effects in Multilayered Pavement System." *Transportation Res. Record: J. Transportation Res. Board*, 342, 39–56.

23. Densit a/s, (2000). Densiphalt® Handbook, Aalborg, Denmark.

24. Diefenderfer, B. K., Al-Qadi, I. L. and Reubush, S. D., (2002). "Prediction of Daily Temperature Profile in Flexible Pavements." Presented at *Transportation Research Board 81st Annual Meeting*, Washington DC, January 2002.

25. Gui, J., Phelan, P. E., Kaloush, K. E., and Golden, J. S., (2007). "Impact of Pavement Thermophysical Properties on Surface Temperatures." *J. Mater. in Civil Eng.*, 19(8), 683–690.

26. Hall, M. & Allinson, D., (2008a). "Assessing the Effects of Soil Grading on the Moisture Content-Dependent Thermal Conductivity of Stabilised Rammed Earth Materials." *Applied Thermal Engineering* 29(4), 740 – 747.

27. Hall, M. & Allinson, D., (2008b). "Assessing the Moisture-Content Dependent Parameters of Stabilised Earth Materials Using the Cyclic-Response Admittance Method." *Energy and Buildings* 40(11), 2044 – 2051.

28. Hermansson, A., (2004). "Mathematical Model for Paved Surface Summer and Winter Temperature: Comparison of Calculated and Measured Temperatures." *Cold Regions Science and Technology*, 40, 1-17.

29. Hermansson, A., (2000). "Simulation Model for Calculating Pavement Temperatures, Including Maximum Temperature." *Transportation Research Record*, 1699, 134-141.

30. Holman, J. P., (2002). "Heat Transfer." McGraw-Hill, New York.

31. Hunter, R. (Ed.), (2003). "The Shell Bitumen Handbook." Thomas Telford, London.

32. Incropera, F. P., DeWitt, D. P., Bergman, T. L. and Lavine, A. S., (2007). "Fundamentals of heat and mass transfer - 6th edition." John Wiley & Sons, USA.

33. ISO, (1996). "8301: 1996 Thermal Insulation – Determination of Steady-State Thermal Resistance and Related Properties – Heat Flow Meter Apparatus." International Organization for Standardization, Genève, Switzerland.

34. Keikha, P., Hall, M. R., and Dawson, A. R., (2010). "Concrete pavements as a source of heating and cooling." Proceedings for the 11th International Symposium on Concrete Roads, 13th – 15th October, Seville, Spain.
35. Lamond, J. F. & Pielert, J. H. (Eds.), (2006). "Significance of Tests and Properties of Concrete and Concrete-Making Materials." ASTM STP 169D, West Conshohocken, PA, USA.
36. Lienhard, I. V. and Lienhard, V., (2006). "A heat transfer text book." Phlogiston Press, Cambridge.
37. Luca, J. & Mrawira, D., (2005). "New Measurement of Thermal Properties of Superpave Asphalt Concrete." *J. Mater. Civil Eng.*, 17(1), 72–79.
38. Marshall, C., Meier, R. W., and Welsh, M., (2001). "Seasonal Temperature Effects on Flexible Pavements in Tennessee." Presented at *Transportation Research Board 80th Annual Meeting*, Washington DC, January 2001.
39. McCullough, B. F. & Rasmussen, R. O., (1998). "Fast track paving: concrete temperature control and traffic opening criteria for bonded concrete overlays Volume I - Final Report." *Technical Report*, Federal Highways Administration, VA, USA.
40. Mehta, P. K. & Monteiro, P. J. M., (2006). "Concrete: Microstructure, Properties, and Materials – Third Edition", McGraw-Hill, USA.
41. Minhoto, M. J. C., Pais, J. C., Pereira, P. A. A., and Picado-Santos, L. G., (2006). "Predicting asphalt pavement temperature with a three-dimensional finite element method." *Journal of the Transportation Research Board*, 96-110.
42. Mohseni, A. & Symons, M., (1998). "Improved AC Pavement Temperature Models from LTPP Seasonal Data." Presented at *Transportation Research Board 77th Annual Meeting*, Washington, DC, January 1998.
43. Mrawira, D. & Luca, J., (2006). "Effect of aggregate type, gradation, and compaction level on thermal properties of hot-mix asphalts." *Canadian. J. of Civil Engineering* 33(11), 1410–1417.
44. Mrawira, D. & Luca, J., (2002). "Thermal Properties and Transient Temperature Response of Full-Depth Asphalt Pavements." *Transportation Res. Record: J. Transportation Res. Board*, 1809
45. (1), 160–171.

46. Niro, N., Shigenobu, M., Nishiwaki, M., and Takeuchi, M., (2009). "Numerical simulation of snow melting on pavement surface with heat dissipation pipe embedded." *Heat Transfer - Asian Res.*, 38(5), 313–329.
47. Palyvos, J. A., (2008). "A survey of wind convection coefficient correlations for building envelope energy systems' modelling." *Applied Thermal Engineering*, 28, 801-808.
48. Ramadhan, R. H. & Wahhab, H. I. A., (1997). "Temperature variation of flexible and rigid pavements in eastern Saudi Arabia." *Building and Environment*, 32(4), 367-373.
49. Ramsey, J. W., Chiang, H. D., and Goldstein, R. J., (1981). "A study of the incoming longwave atmospheric radiation from a clear sky." *Journal of Applied Meteorology*, 21, 566-578.
50. RETScreen, (2005). "Clean Energy Project Analysis: RETScreen Engineering & Cases Textbook." Minister of Natural Resources Canada, ISBN: 0-662-39191-8.
51. Rosenfeld, A. H., Akbari, H., Romm, J. J., and Pomerantz, M., (1998). "Cool Communities: Strategies for Heat Island Mitigation and Smog Reduction." *Energy and Buildings*, 28(1), 51-62.
52. Setyawan, A., (2003). "Development of Semi-Flexible Heavy-Duty Pavements" *PhD thesis*, University of Leeds, UK.
53. Solaimanian, M. & Bolzan, P., (1993). "Analysis of the Integrated Model of Climatic Effects on Pavements." Technical report SHRP-A-637.
54. Solaimanian, M. & Kennedy, T. W., (1993). "Predicting Maximum Pavement Surface Temperature Using Maximum Air Temperature and Hourly Solar Radiation." *Transportation Research Record*, 1417, 1-11.
55. Underwood, C. P. & Yik, F. W. H., (2004). "Modelling methods for energy in buildings." Blackwell publishing, Oxford.
56. US Department of Transportation – Federal Transport Administration, (2009). "LTPP Seasonal Monitoring Programme (SMP): Pavement Performance Database (PPDB)." [electronic database], Standard Data Release 23.0, DVD Version, USA.
57. van Bijsterveld, W. T. and de Bondt, A. H., (2002). "Structural Aspects of Asphalt Pavement Heating and Cooling Systems." *Third International Symposium on 3D Finite Element Modelling, Design and Research*, 2nd – 5th April 2002, Amsterdam, Netherlands.

58. Vehrencamp, J., (1953). “Experimental Investigation of Heat Transfer at an Air-earth Interface.” *Trans. Amer. Geophys. Union*, 34, 22–29.

59. Yavuzturk, C., Ksaibati, K., and Chiasson, A. D., (2005). “Assessment of Temperature Fluctuations in Asphalt Pavements Due to Thermal Environmental Conditions Using a Two-Dimensional, Transient Finite-Difference Approach.” *J. Mater. in Civil Eng.*, 17(4), 465–475.

60. Yun, T. S. & Santamarina, J. C., (2008). “Fundamental Study of Thermal Conduction in Dry Soils, *Granular Matter*.” 10(3), 197-207.

61. Zapata, C. E. & Houston, W. N., (2008). “Calibration and Validation of the Enhanced Integrated Climatic Model for Pavement Design.” NCHRP Report 602, Transportation Research Board, Washington, D.C.

Figure 1
Click here to download high resolution image

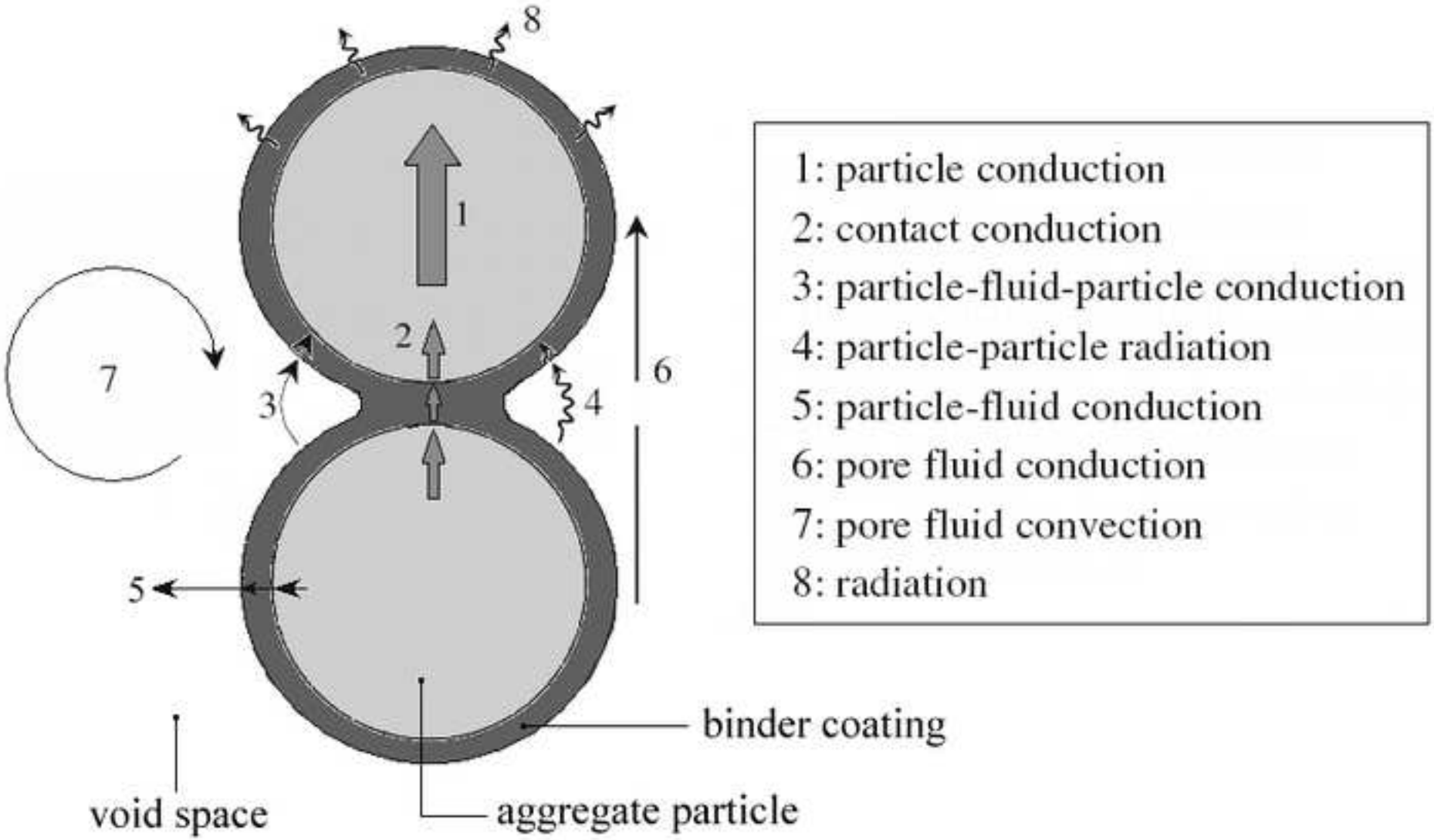

Figure 2

Click here to download high resolution image

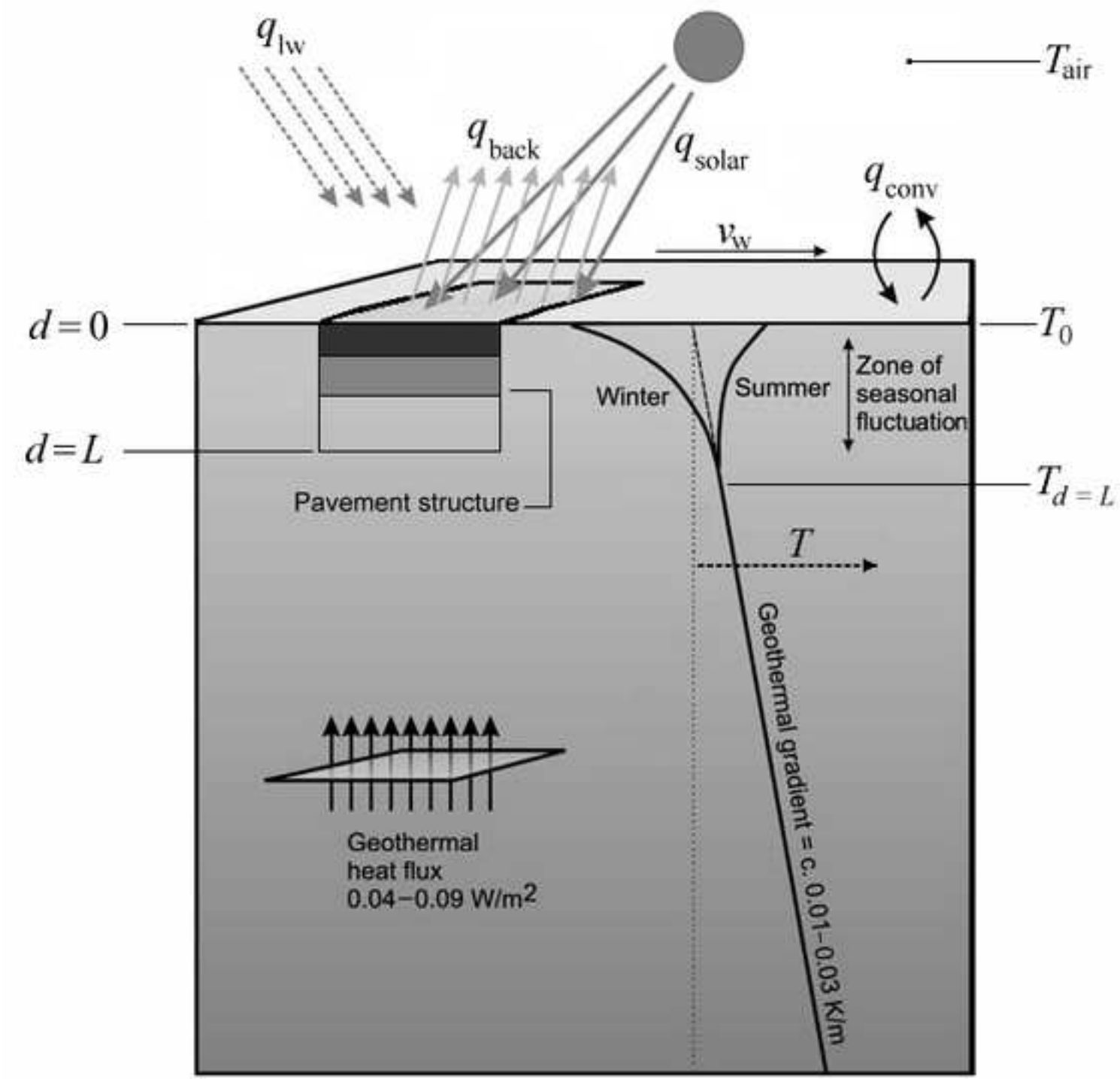

Figure 3

Click here to download high resolution image

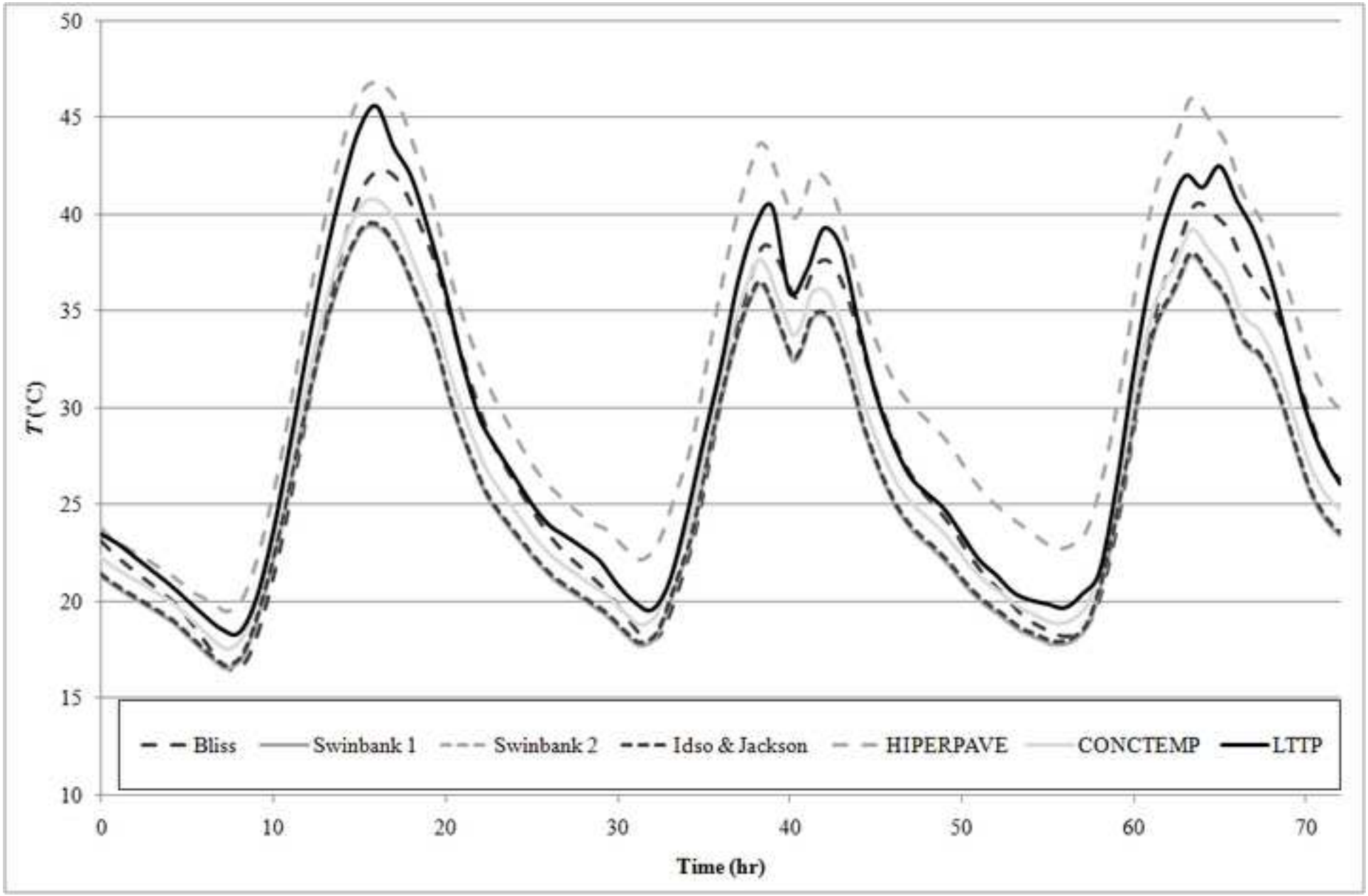

Figure 4

Click here to download high resolution image

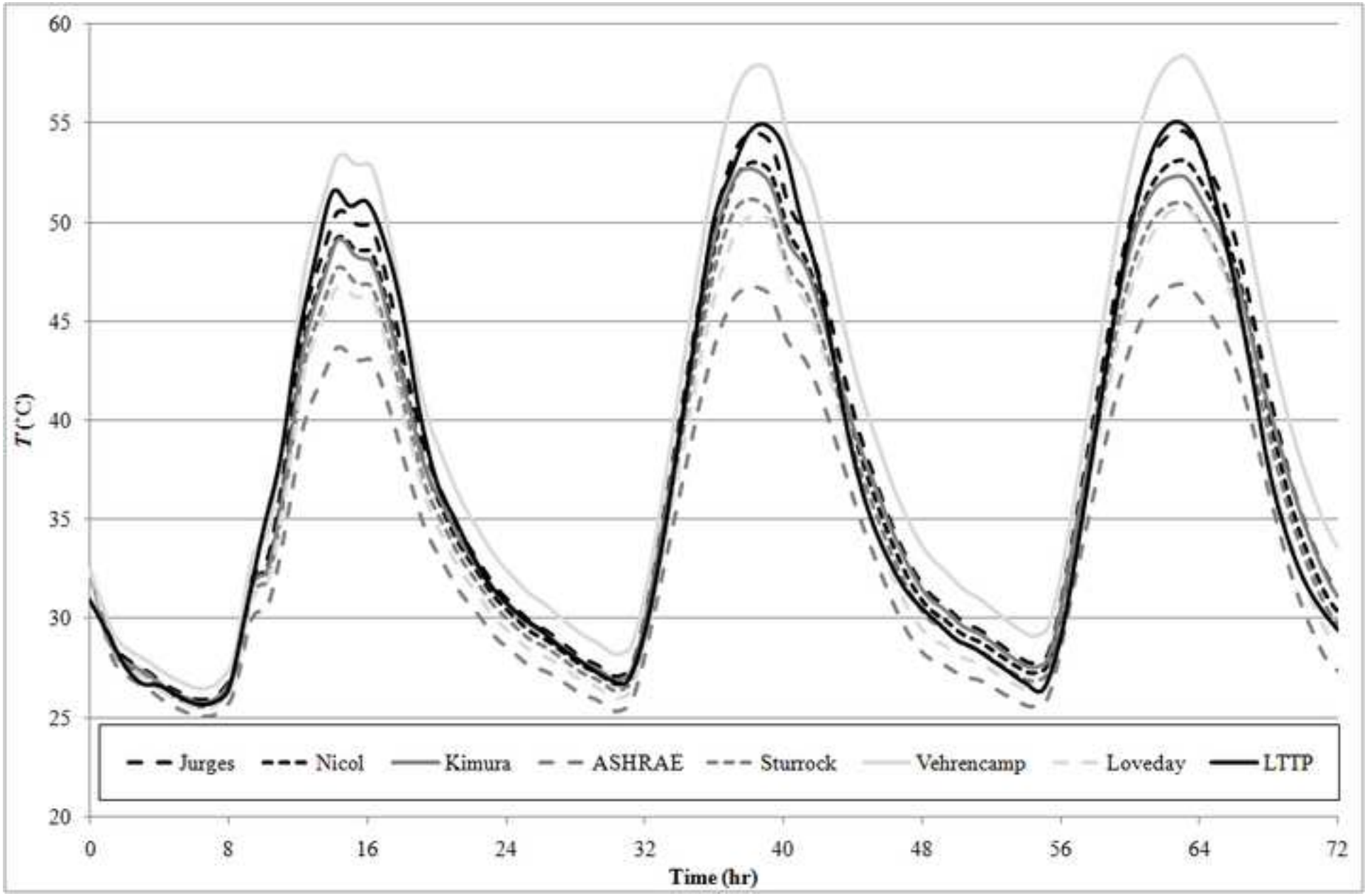

Figure 5
Click here to download high resolution image

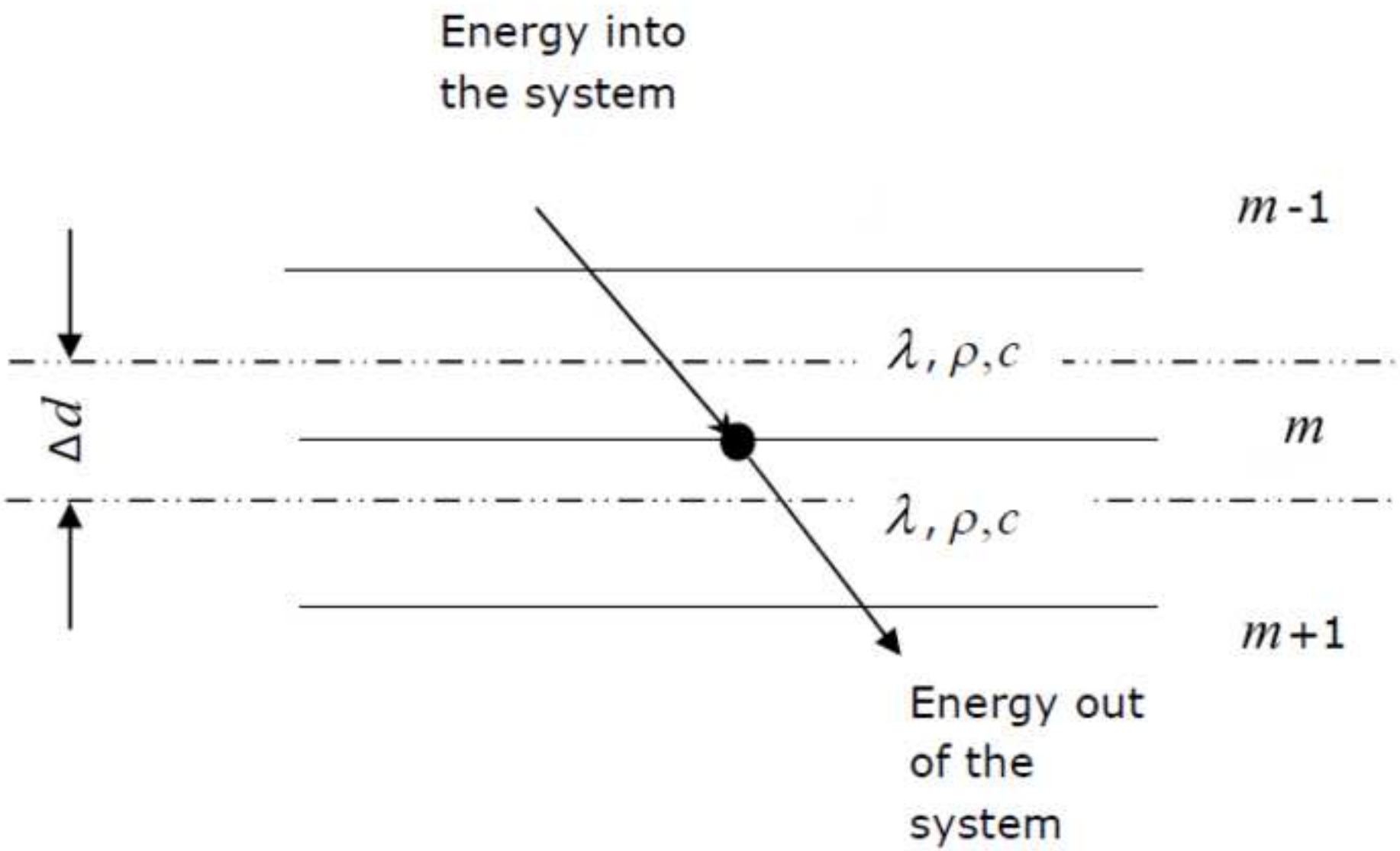

Figure 6

Click here to download high resolution image

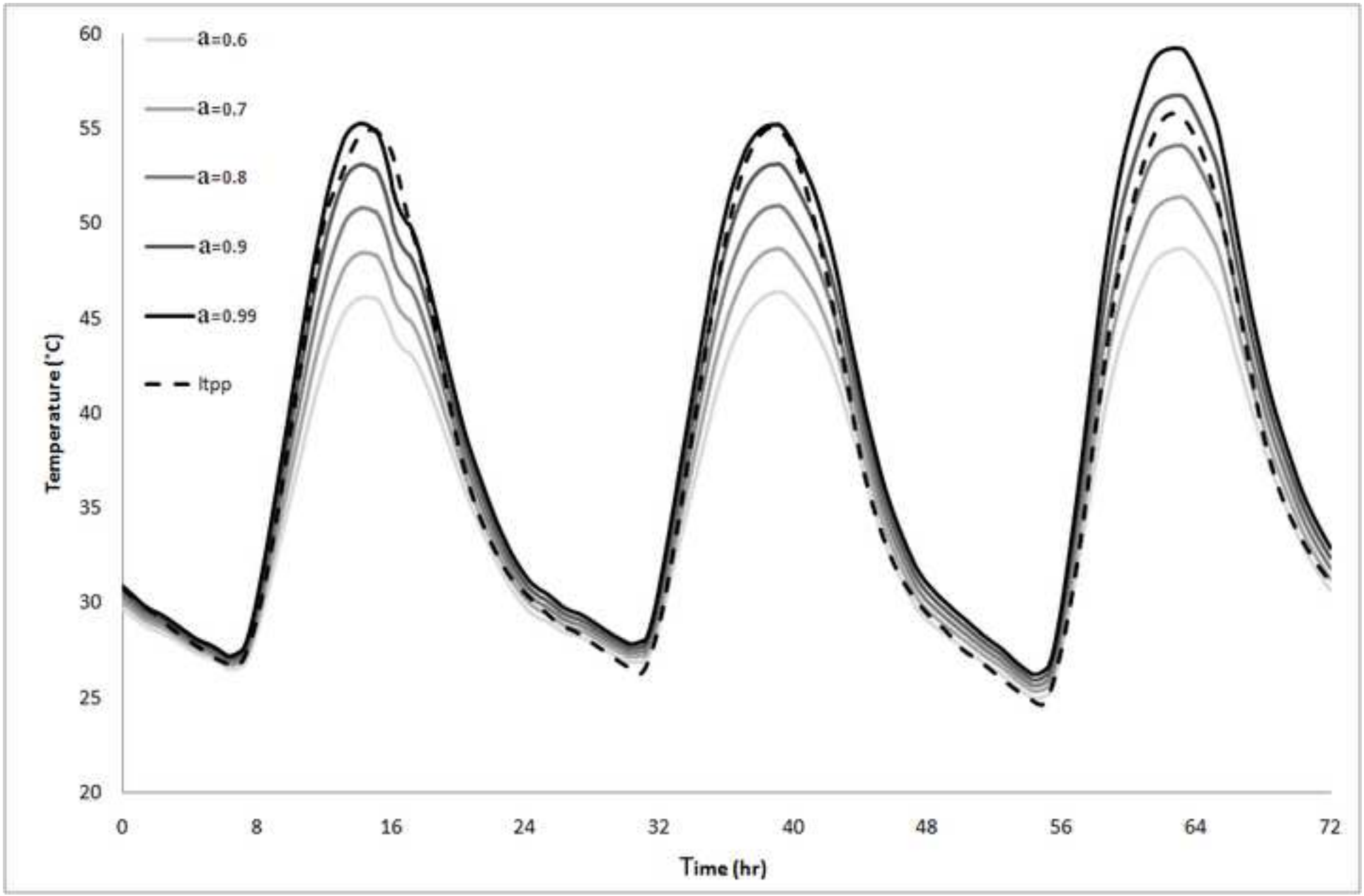

Figure 7

Click here to download high resolution image

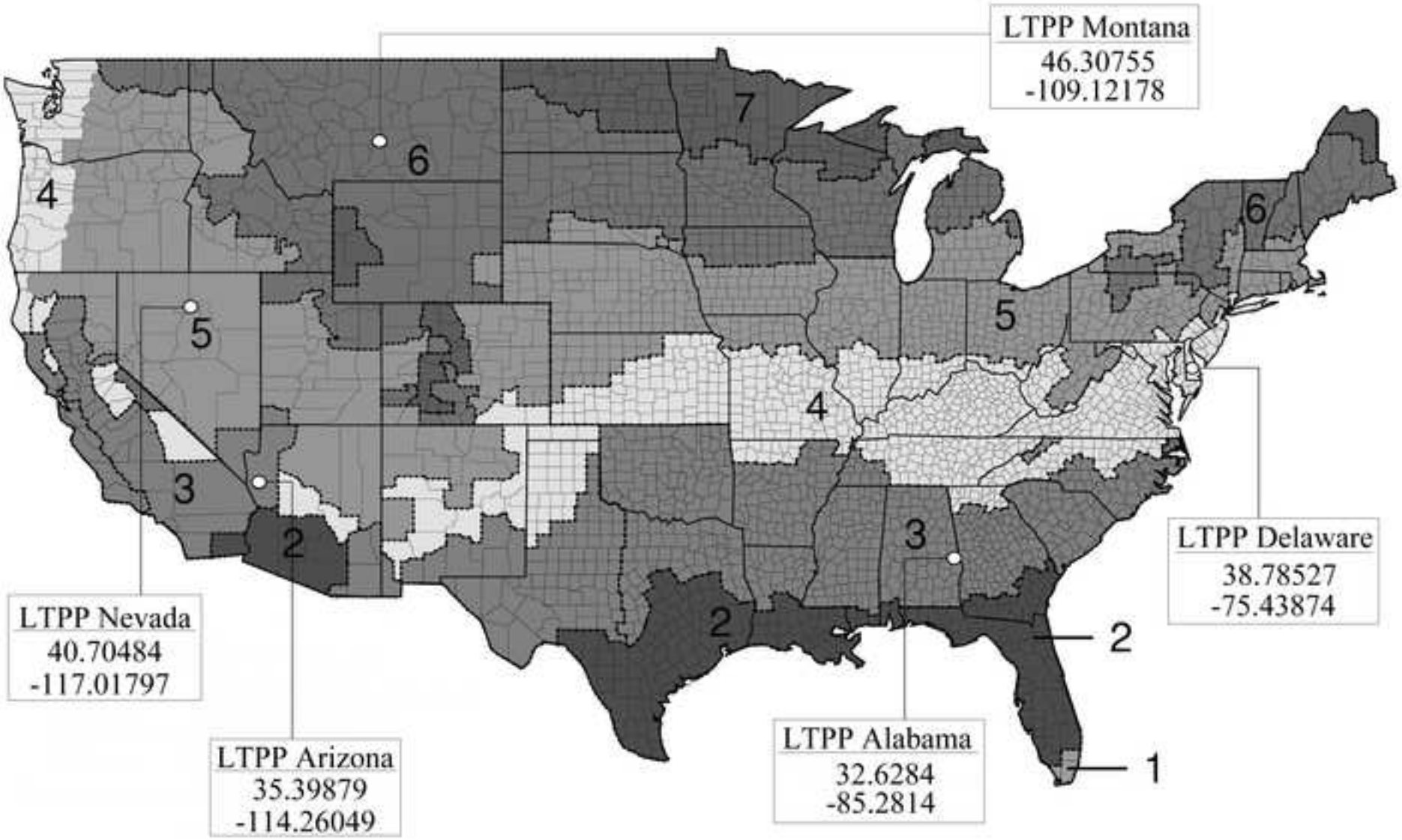

Figure 8

Click here to download high resolution image

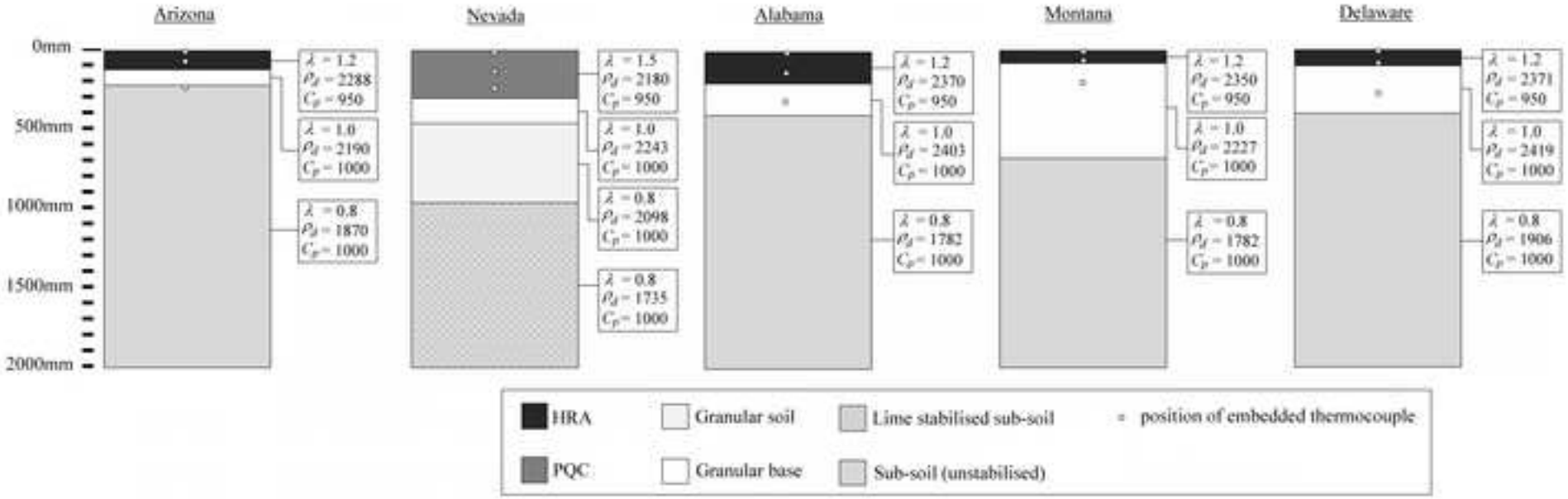

Figure 9

Click here to download high resolution image

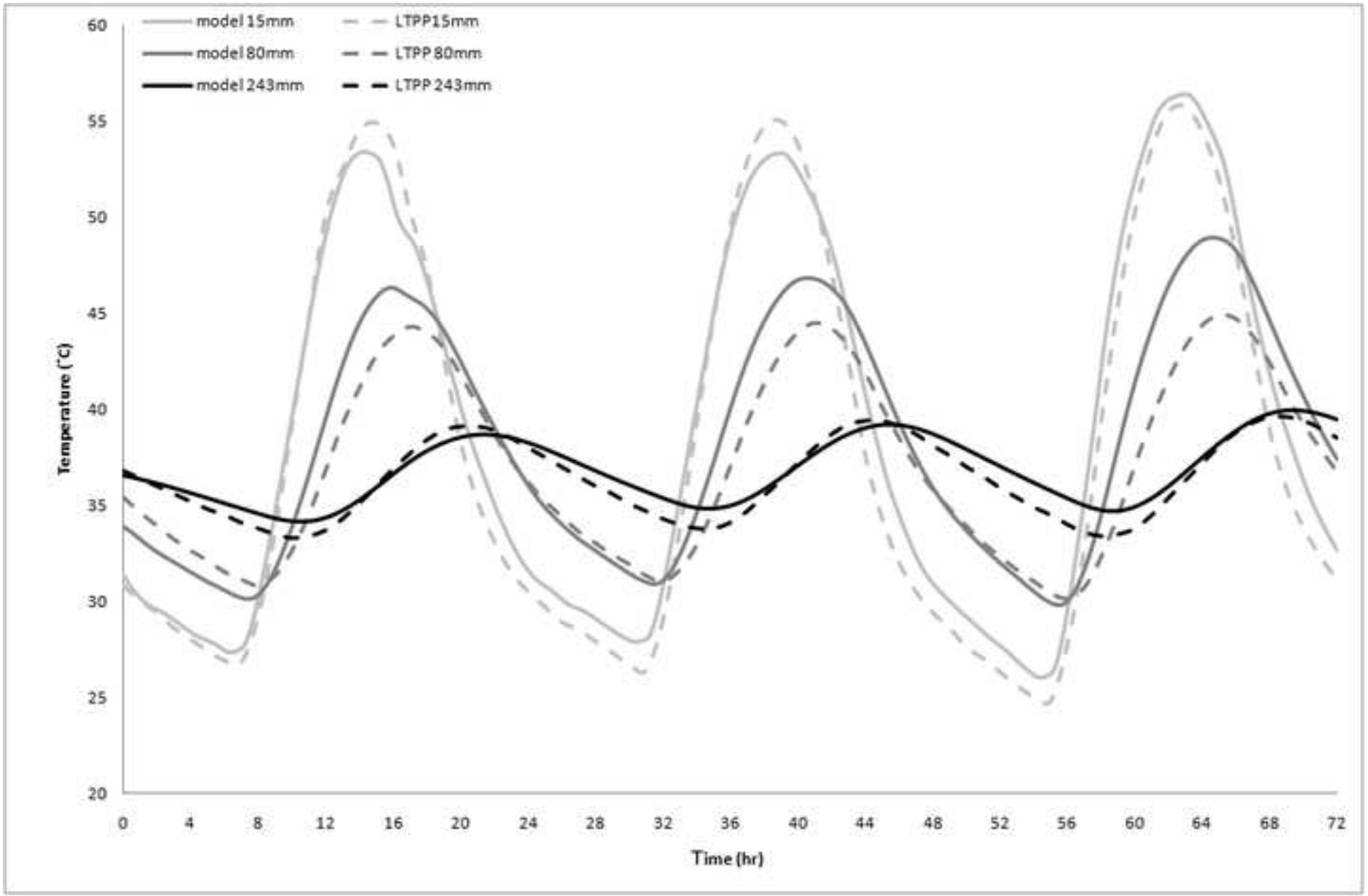

Figure 10

Click here to download high resolution image

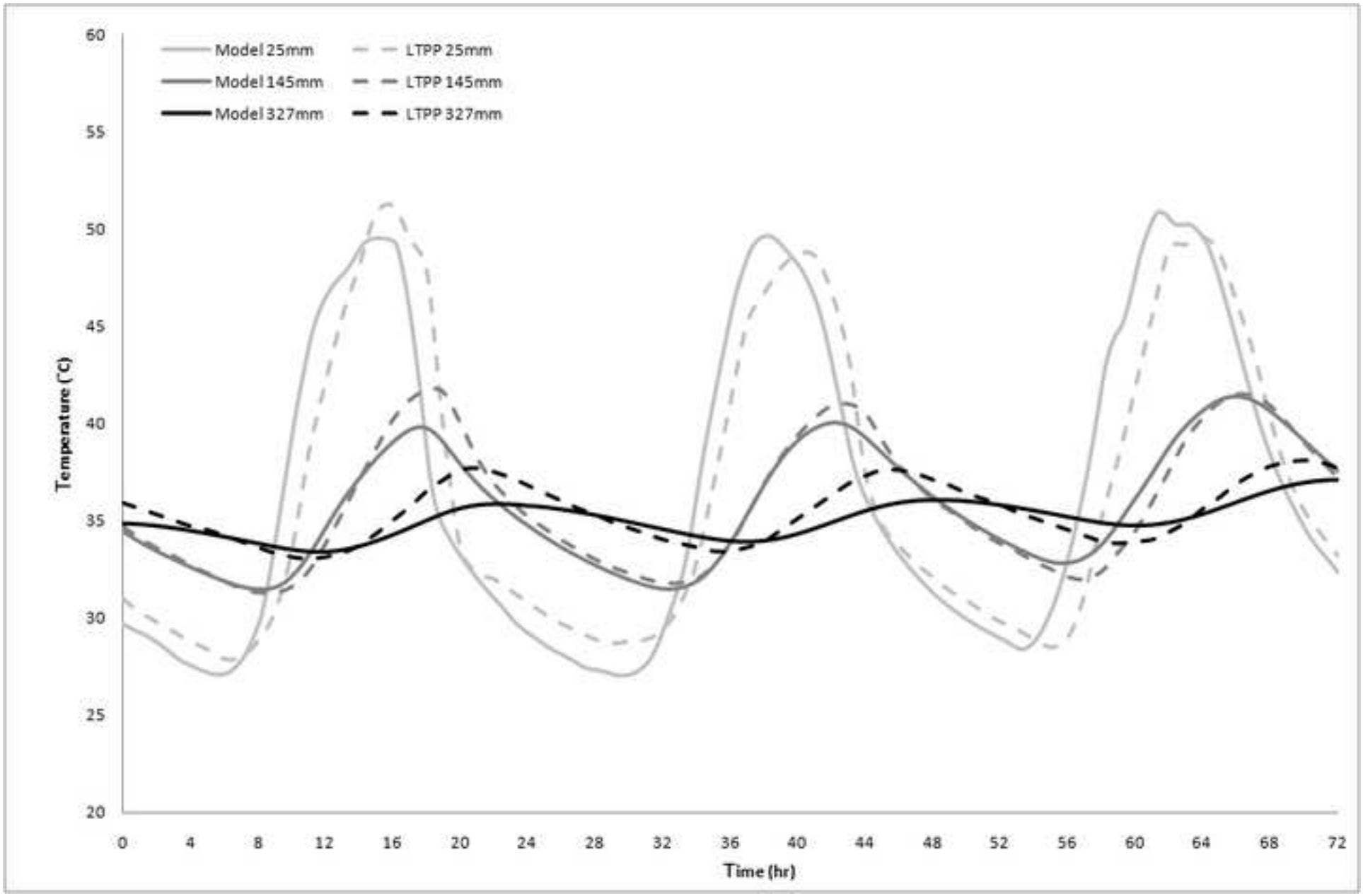

Figure 11

Click here to download high resolution image

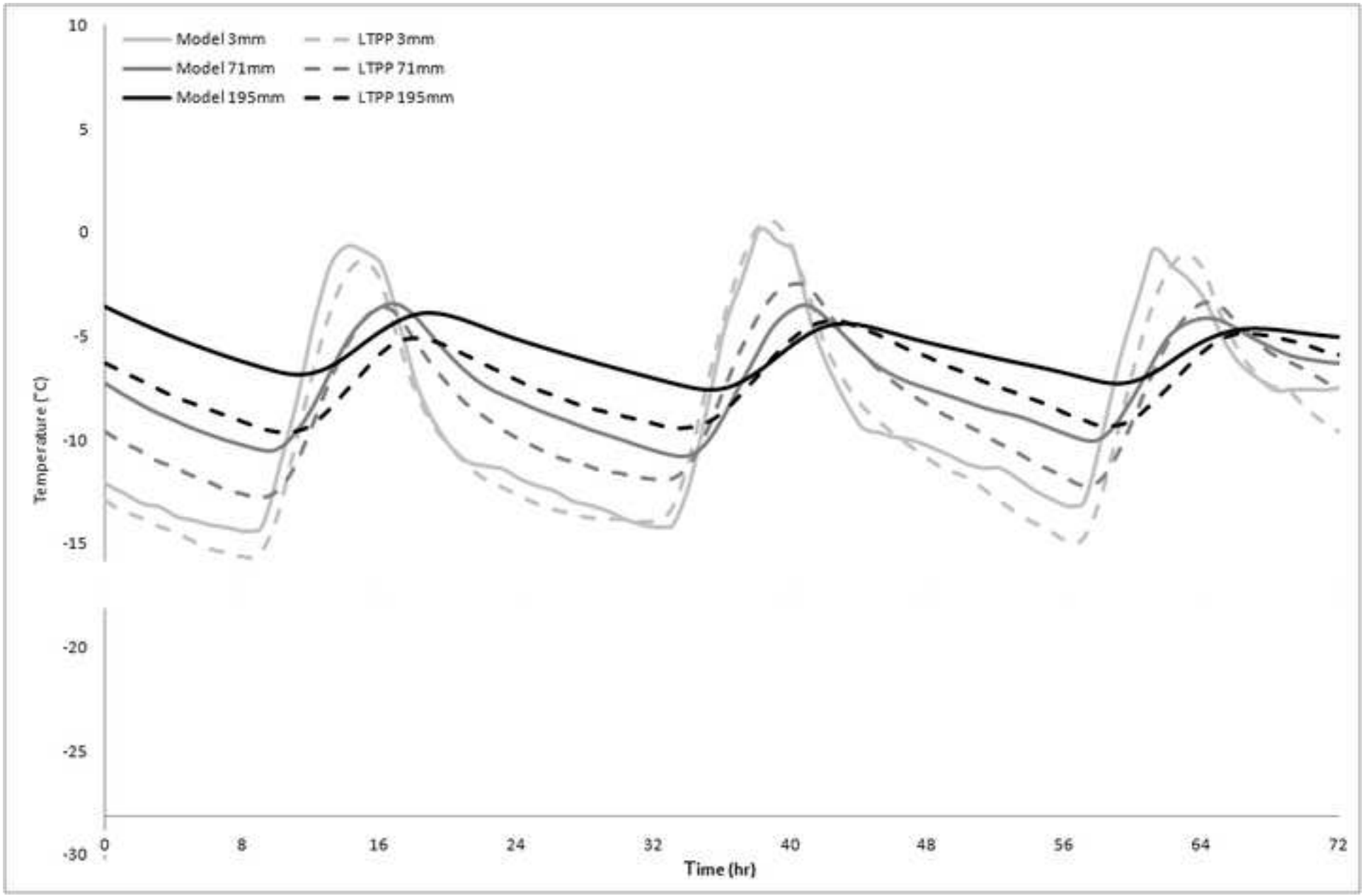

Figure 12

Click here to download high resolution image

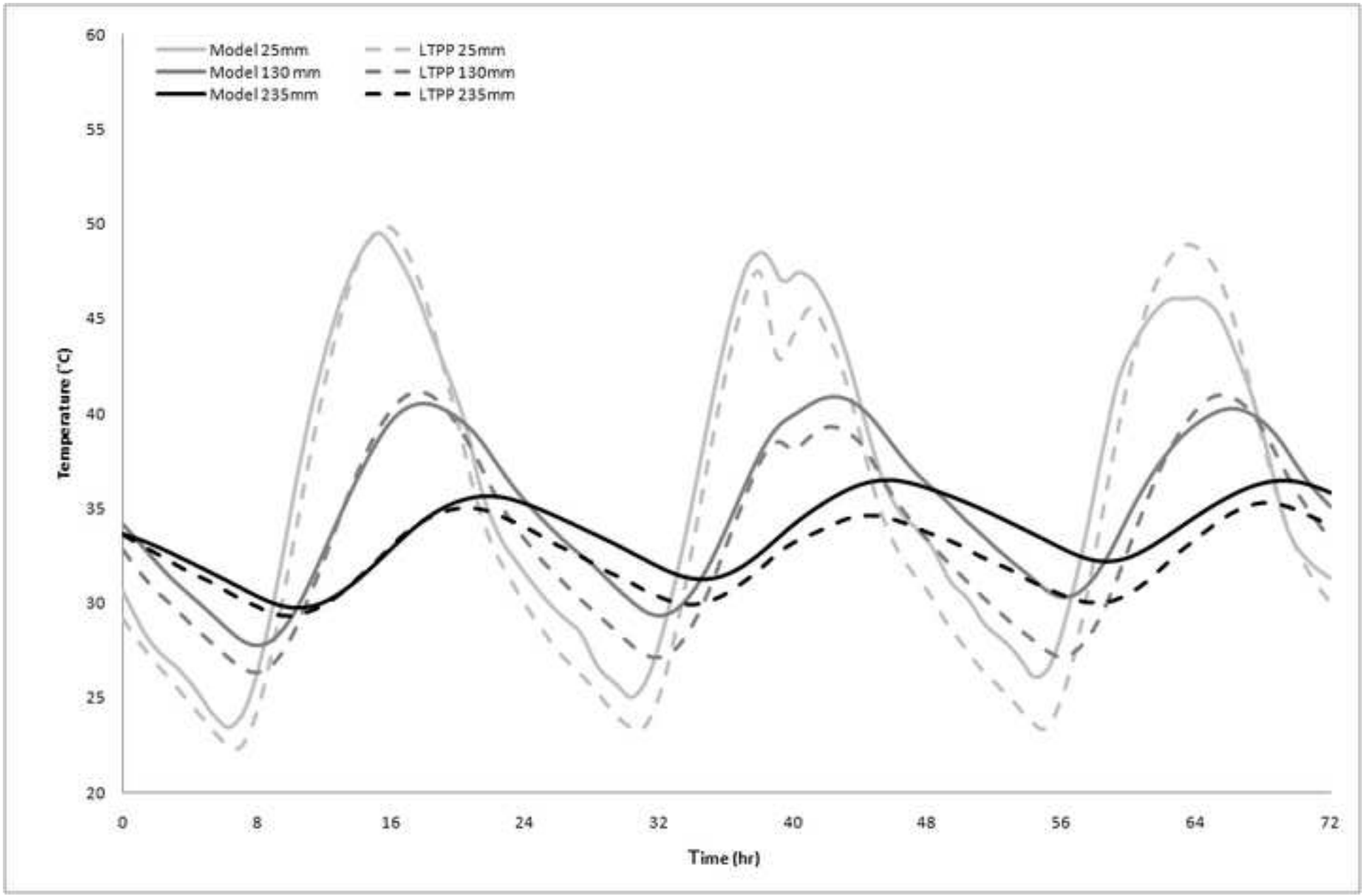

Figure 13

Click here to download high resolution image

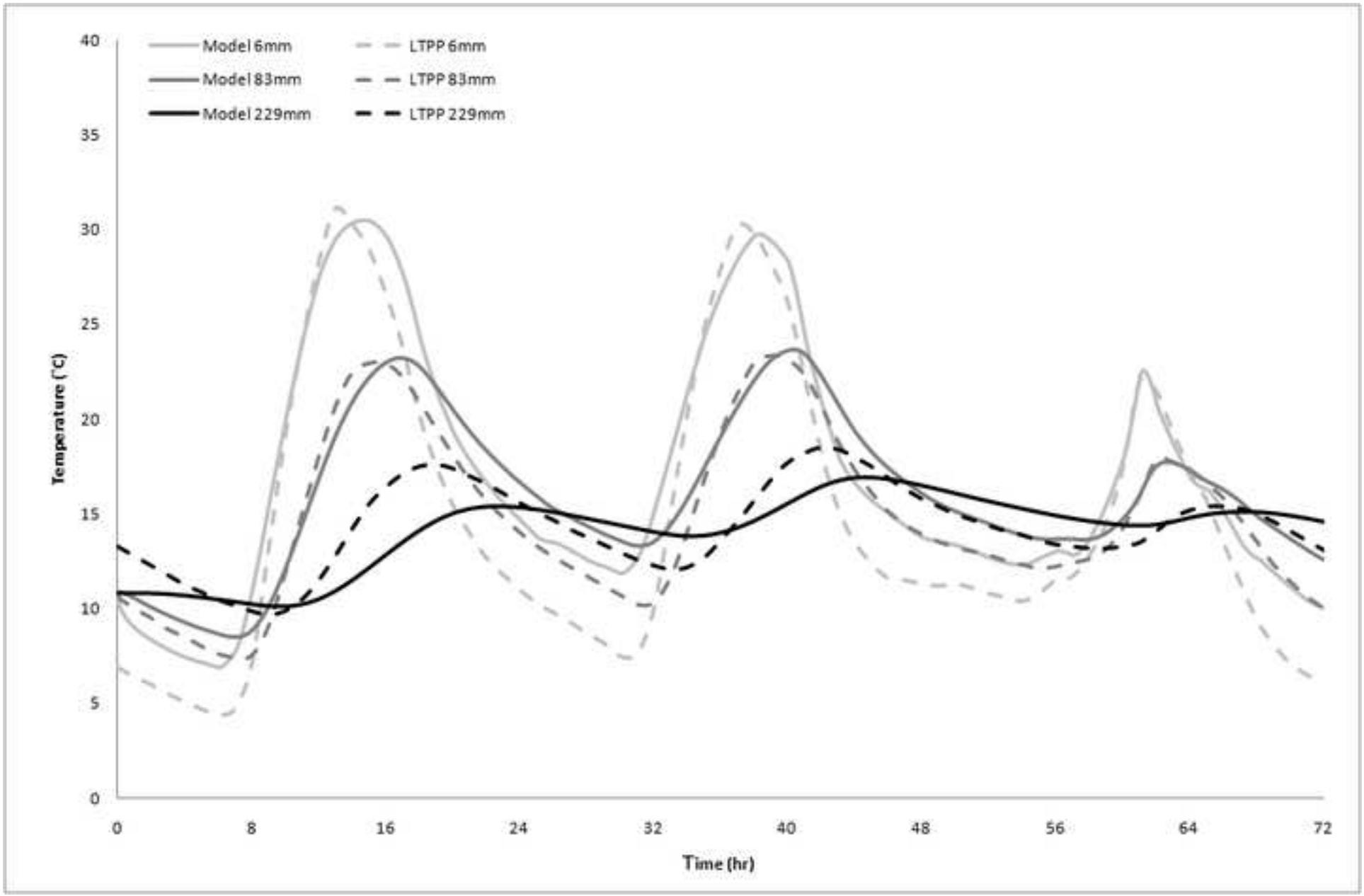

Figure 14
Click here to download high resolution image

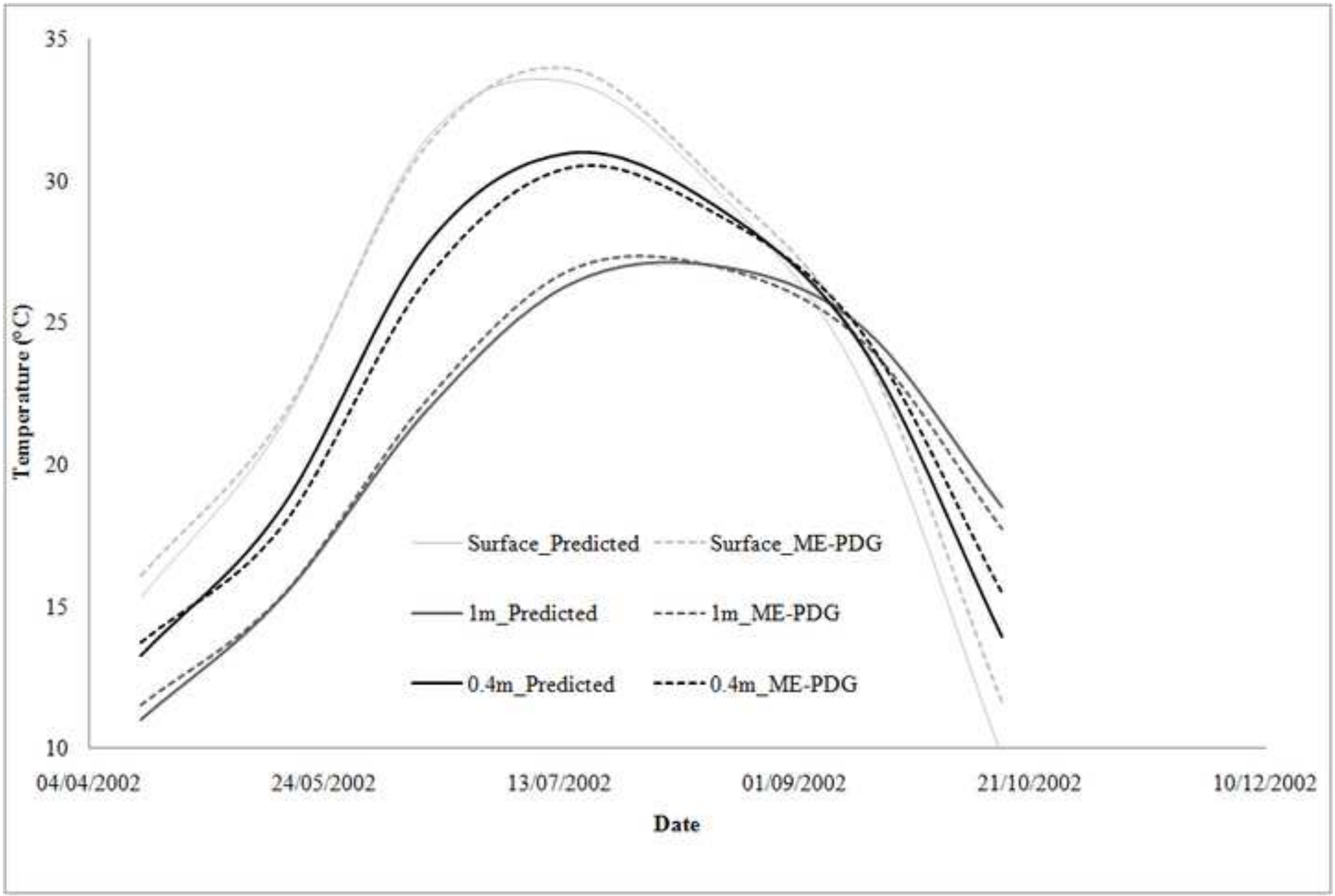

Figure 15
Click here to download high resolution image

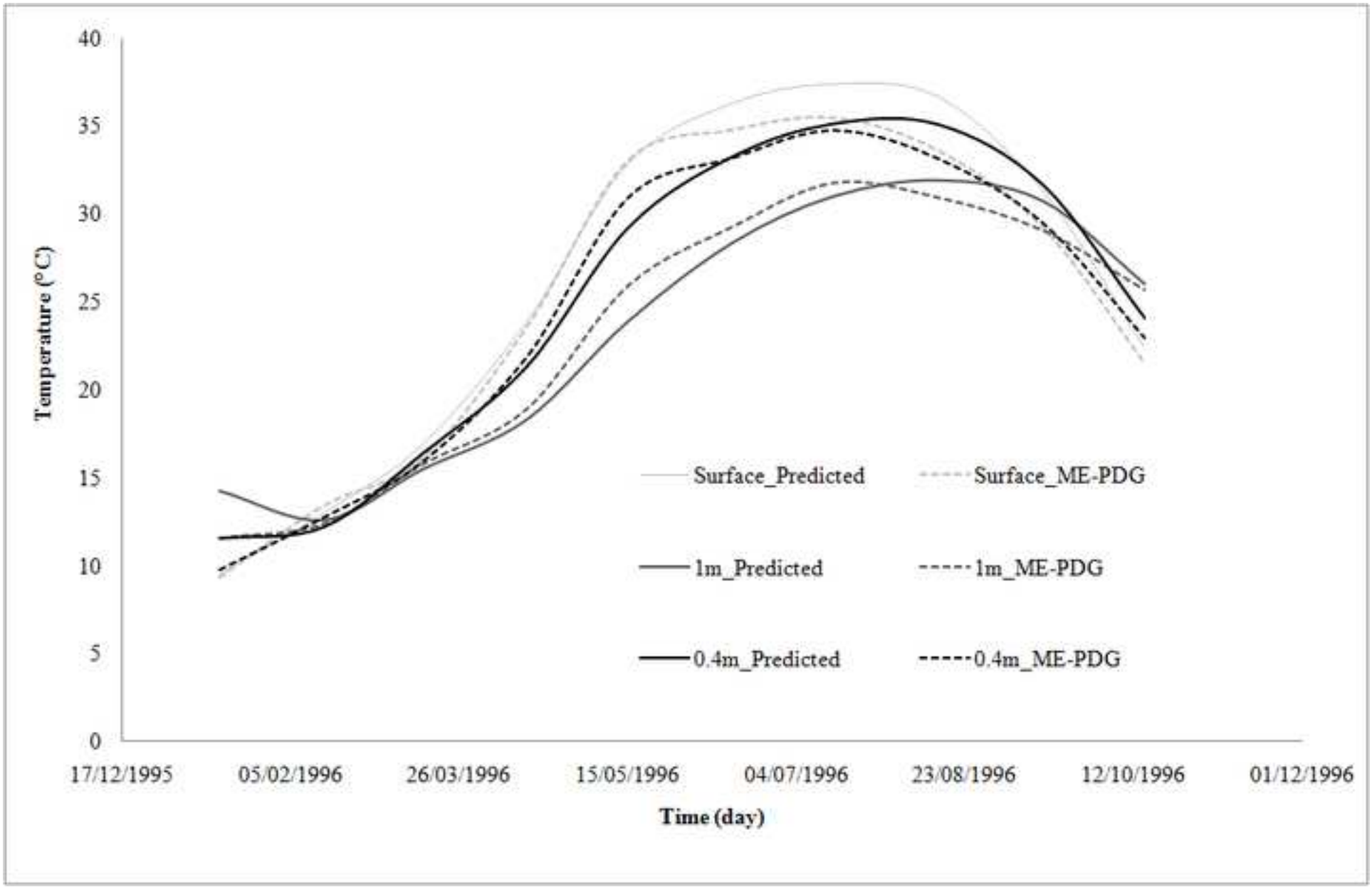

Figure 16

Click here to download high resolution image

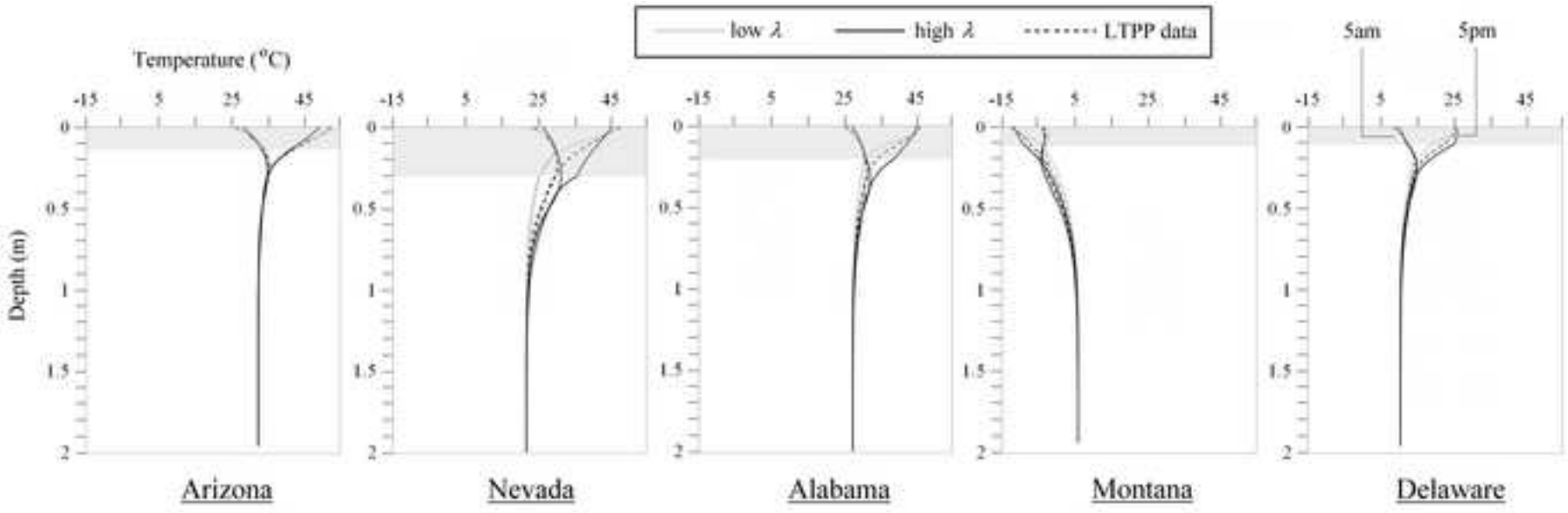

Figure 17

Click here to download high resolution image

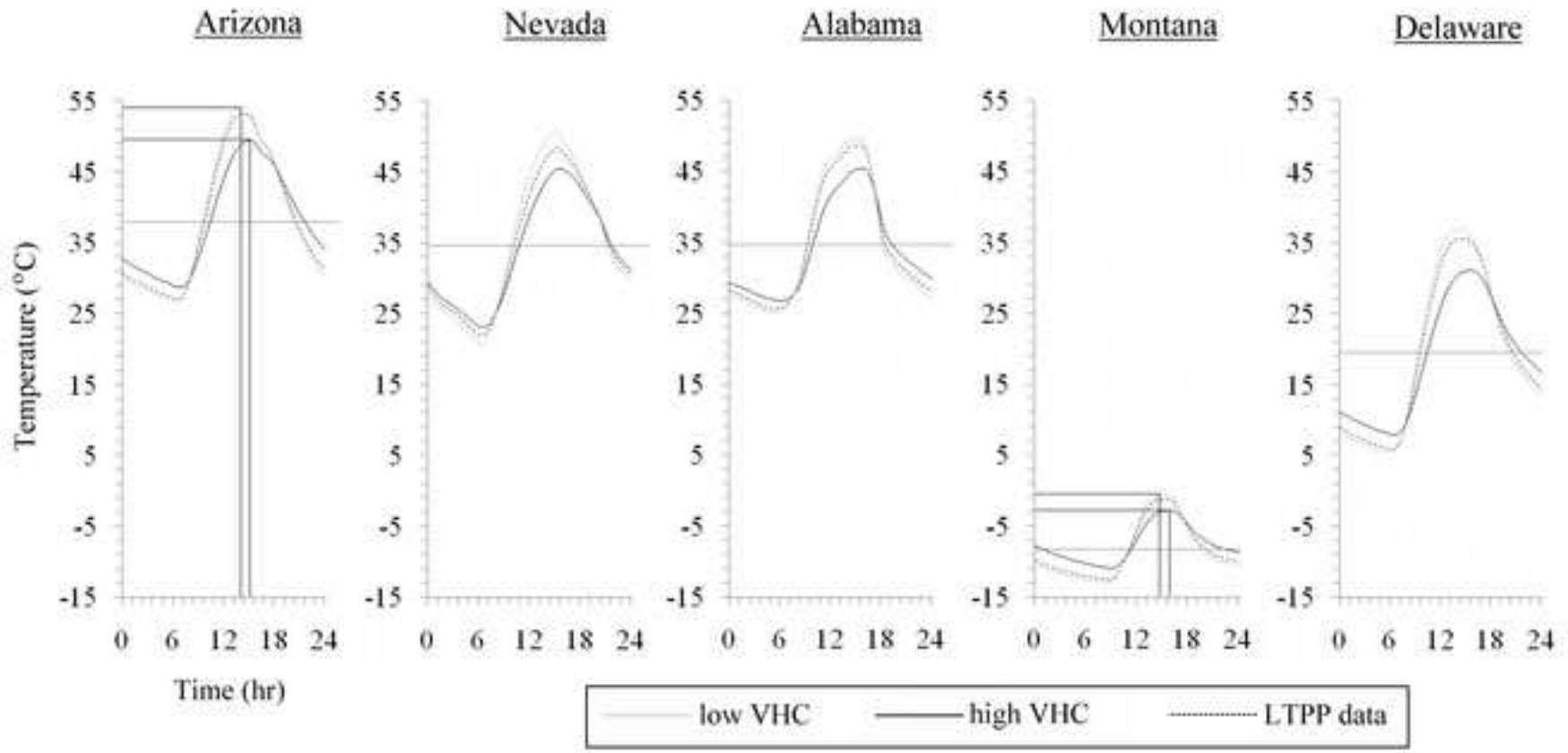

Figure 18
Click here to download high resolution image